Available online at www.sciencedirect.com
SCIENCE DIRECT
Biochemical Pharmacology 69 (2005) 669–678
Biochemical Pharmacology
www.elsevier.com/locate/biochempharm

Assignment of voltage-gated potassium channel blocking activity to κ-KTx1.3, a non-toxic homologue of κ-hefutoxin-1, from *Heterometrus spinifer* venom

Selvanayagam Nirthanan[a,1], Joost Pil[b,1], Yousra Abdel-Mottaleb[b], Yuko Sugahara[c], Ponnampalam Gopalakrishnakone[d,*], Jeremiah S. Joseph[e], Kazuki Sato[c], Jan Tytgat[b]

[a]*Department of Neurobiology, Harvard Medical School, Boston, MA 02115, USA*
[b]*Laboratory of Toxicology, University of Leuven, 3000 Leuven, Belgium*
[c]*Fukuoka Women's University, Kasumigaoka, Higashi-ku, Fukuoka 813-8529, Japan*
[d]*Venom and Toxin Research Programme, Faculty of Medicine, National University of Singapore, Singapore 117597, Singapore*
[e]*The Scripps Research Institute, La Jolla, CA 92037, USA*

Received 19 July 2004; accepted 20 October 2004

Abstract

A new family of weak K^+ channel toxins (designated κ-KTx) with a novel "bi-helical" scaffold has recently been characterized from *Heterometrus fulvipes* (Scorpionidae) venom. Based on the presence of the minimum functional dyad (Y5 and K19), κ-hefutoxin-1 (κ-KTx1.1) was investigated and found to block Kv 1.2 (IC_{50} ~40 μM) and Kv 1.3 (IC_{50} ~150 μM) channels. In the present study, κ-KTx1.3, that shares ~60% identity with κ-hefutoxin 1, has been isolated from *Heterometrus spinifer* venom. Interestingly, despite the presence of the functional dyad (Y5 and K19), κ-KTx1.3 failed to reproduce the K^+ channel blocking activity of κ-hefutoxin-1. Since the dyad lysine in κ-KTx1.3 was flanked by another lysine (K20), it was hypothesized that this additional positive charge could hinder the critical electrostatic interactions known to occur between the dyad lysine and the Kv 1 channel selectivity filter. Hence, mutants of κ-KTx1.3, substituting K20 with a neutral (K20A) or a negatively (K20E) or another positively (K20R) charged amino acid were synthesized. κ-KTx1.3 K20E, in congruence with κ-hefutoxin 1 with respect to subtype selectivity and affinity, produced blockade of Kv 1.2 ($IC_{50} = 36.8 \pm 4.9$ μM) and Kv 1.3 ($IC_{50} = 53.7 \pm 6.7$ μM) but not Kv 1.1 channels. κ-KTx1.3 K20A produced blockade of both Kv 1.2 ($IC_{50} = 36.9 \pm 4.9$ μM) and Kv 1.3 ($IC_{50} = 115.7 \pm 7.3$ μM) and in addition, acquired affinity for Kv 1.1 channels ($IC_{50} = 110.7 \pm 7.7$ μM). κ-KTx1.3 K20R failed to produce any blockade on the channel subtypes tested. These data suggest that the presence of an additional charged residue in a position adjacent to the dyad lysine impedes the functional block of Kv 1 channels produced by κ-KTx1.3.

Keywords: Scorpion toxin; Voltage-gated potassium channel; Functional dyad; κ-Hefutoxin 1; κ-KTx1.3; *Heterometrus spinifer*

The venoms of the black scorpion *Heterometrus* spp. (Scorpionidae) including the Malaysian black scorpion (*Heterometrus spinifer*) have been reported to be of a lower order of toxicity in comparison to those from the Buthidae scorpions [1] from which highly potent neurotoxins that target Na^+ as well as various subtypes of K^+ channels have been isolated [2]. In contrast, mostly neurotoxins which modify K^+ channel activity, the role of which is presumed to be of minor consequence in lethal envenomation, have been found to be present in low quantities in the venoms of some Scorpionidae members [3–5]. Scorpion toxins that target K^+ channels are compact peptides that typically contain 23–43 amino acid residues and three or four disulfide bridges [2,6,7]. Moreover, almost all of these toxins adopt a highly conserved

Abbreviation: K^+, potassium

* Corresponding author. Tel.: +65 687 43207; fax: +65 677 87643.
E-mail address: antgopal@nus.edu.sg (P. Gopalakrishnakone).
[1] Contributed equally to this work.

0006-2952/$ – see front matter © 2004 Elsevier Inc. All rights reserved.
doi:10.1016/j.bcp.2004.10.018

secondary structure, the cysteine-stabilized α/β-fold, which consists of a segment of an α-helix and a double- or triple-stranded β-sheet that are held together in a stable conformation by two or more disulfide bridges [2,7–10]. These toxins have been classified into three-subfamilies, called α-, β- and γ-KTxs [10–12].

We have recently reported the isolation and characterization of a 22-residue long peptide with weak K^+ channel blocking activity (IC_{50} ~40 to 150 μM), κ-hefutoxin 1, from *Heterometrus fulvipes* venom that adopts a novel fold comprising of two parallel α-helices cross-linked by two disulfide bridges [13]. Interestingly, the K^+ channel blocking activity of κ-hefutoxin 1 was deduced following its structural characterization that revealed the presence of two key residues, tyrosine and lysine at positions 5 and 19, respectively, positioned at a distance of ~6.0 Å between the lysine's α-carbon and the center of the aromatic face of the tyrosine [13]. Such a critically positioned dyad, composed of a positively charged amino acid and a hydrophobic residue, is well-known to constitute the minimum functional requirement for K^+ channel blocking activity of a variety of toxins isolated from venoms across different phyla [13–15].

We have now isolated a new 23-residue peptide from the venom of *H. spinifer* that shares ~60% identity with κ-hefutoxin 1, and based on sequence similarity, was identified as the third member of the κ-KTx subfamily and hence designated as κ-KTx1.3. However, despite the presence of the putative functional dyad (Y5 and K19) in identical positions in its sequence, κ-KTx1.3 failed to reproduce the blocking activity of κ-hefutoxin 1 on Kv 1.2 and Kv 1.3 channels. On analyzing the primary structure of κ-KTx1.3, it was found that the critical lysine (K19) was flanked by another lysine (K20) and it was postulated that this additional positive charge may hinder critical electrostatic interactions reported to occur between the dyad lysine extremity and the carbonyl oxygen atoms of conserved residues in the Kv 1 channel selectivity filter. We have therefore, chemically synthesized mutants of κ-KTx1.3 substituting the flanking lysine with a neutral amino acid (K20A) or a negatively charged glutamic acid (K20E) as found in κ-hefutoxin 1. Interestingly, by these single-residue substitutions, we were able to assign K^+ channel blocking activity to a scorpion venom-derived peptide that was otherwise inactive on Kv channels.

1. Materials and methods

1.1. Materials

H. spinifer venom was extracted from live scorpions maintained in captivity in the Venom and Toxin Research Laboratory, National University of Singapore as described previously [16]. Pre-packed chromatography columns were purchased from Pharmacia Biotech. All drugs and chemicals were purchased from Sigma Chemicals with the exception of the following, which were obtained from the sources indicated: reagents for N-terminal sequencing, acetonitrile (Fisher Scientific) and trifluoroacetic acid (Fluka Chemika-Biochemika). HPLC-grade water was obtained by using a Milli-Q purification system (Millipore).

1.2. Purification of κ-KTx1.3

Pooled scorpion venom was subjected to ultra-filtration using Mr = 5000 micro-concentrators (Amicon). The venom (500 μl) was transferred to the sample reservoir of the microconcentrator and centrifuged at 4500 × *g* for 90 min at 4 °C. The filtrate of Mr < 5000 was then subjected to a single-step reverse phase HPLC using a Sephasil C8 (0.21 cm × 10 cm) column using a Vision Biocad Workstation (Bio-Rad Laboratories). The column was equilibrated with 0.1% trifluoroacetic acid and the proteins were eluted with a linear gradient (20–50% over 80 min) of eluant (80% acetonitrile in 0.1% trifluoroacetic acid). Elution of proteins was monitored at 215 nm.

1.3. Mass spectrometry

Purified κ-KTx1.3 was subjected to electrospray ionization mass spectrometry as described previously [16] using a Perkin-Elmer Sciex API 300 triple quadrupole instrument (Sciex) equipped with an ion-spray interface. The ion-spray and orifice voltages were set to 4600 and 30 V, respectively. Nitrogen was used as curtain gas with a flow rate of 0.6 l/min while compressed air was used as a nebulizer gas. The sample was infused by flow injection at a flow rate of 50 μl/min using Shimadzu 10 AD pumps as the solvent delivery system. Matrix-assisted laser desorption ionisation–time of flight (MALDI–TOF) mass spectrometry was performed on a Voyager DE-STR Biospectrometry Workstation (Applied Biosystems). Saturated sinapinic acid (3,5-dimethoxy-4-hydroxycinnamic acid) (10 mg/ml) in 1:1 acetonitrile:water containing 0.3% trifluoroacetic acid was used as the matrix. The sample (~5 pmol in 1 μl) was spotted onto a stainless steel sample plate with 1 μl of matrix solution and dried off. Molecular ions were generated using a nitrogen laser (337 nm) at an intensity of 1800–2200 and extraction of ions was delayed by 800 ns. The accelerating voltage was set at 25,000 V and the grid and guide wire voltages at 93.0 and 0.3%, respectively. The spectrum was calibrated using external standards.

1.4. Determination of the N-terminal amino acid sequence

Amino terminal sequencing of the native and pyridylethylated protein was done by automated Edman degrada-

tion using a Perkin-Elmer Applied Biosystems 494 pulsed-liquid phase protein sequencer (Procise) with an on-line 785A phenylthiohydantoin-derivative analyzer. For pyridylethylation, native κ-KTx1.3 was re-suspended in 100 μl of denaturant buffer (6.0 M guanidinium hydrochloride, 0.13 M Tris, 1 mM EDTA, pH 8.0) containing 0.07 M β-mercaptoethanol and heated at 37 °C for 2 h. Subsequently, 1.5-fold molar excess (over sulfhydryl groups) of 4-vinylpyridine was added and incubated at room temperature for 2 h, after which the sample was desalted by reverse phase HPLC.

1.5. Peptide synthesis

Linear precursors of κ-KTx1.3 with free (κ-KTx1.3(OH)) and amidated (κ-KTx1.3(NH_2)) carboxy terminals as well their analogues (κ-KTx1.3 K20A, κ-KTx1.3 K20E and κ-KTx1.3 K20R) were synthesized by solid phase methodology with Fmoc chemistry on an Applied Biosystems (model 433A) peptide synthesizer, oxidized by air oxidation and purified by HPLC as described previously [13]. The structures and purity of the synthetic peptides and native κ-KTx1.3 were confirmed by HPLC co-injection analysis and MALDI–TOF mass spectrometry measurements. In order to determine the disulfide pairings, synthetic κ-KTx1.3(OH) (0.4 mg) was dissolved in 0.4 ml of 0.1 M phosphate buffer pH 6.5) and digested with trypsin (0.1 mg at 37 °C for 3 h). The digested peptide fragments were separated by HPLC and subjected to MALDI–TOF mass spectrometry measurements.

1.6. Molecular modeling

The NMR structure of κ-hefutoxin 1 (PDB accession number 1HP9; first out of the ensemble of 20 lowest energy structures) from *H. fulvipes* was used as the template for comparative molecular modeling of κ-KTX1.3. The molecular model was constructed using InsightII (Molecular Simulations Inc., USA) as described previously [17].

1.7. Expression in Xenopus oocytes

Kv 1.1 (rat), Kv 1.2 (rat) and Kv 1.3 (human) channels were studied. Plasmids containing Kv 1.1 were first linearized with PstI (New England Biolabs) 3′ to the 3′ non-translated β-globin sequence in a custom-made high expression vector for oocytes, pGEM-HE [18] and then transcribed using Ambion's mMESSAGE mMachine T7 transcription kit (Ambion). The cDNA encoding Kv 1.2 in its original vector, pAKS2, was first subcloned into pGEM-HE [18]. The insert was released by double restriction digest with *Bgl*II and *Eco*RI and ligated into the *Bam*HI and *Eco*RI sites of pGEM-HE. For in vitro transcription, the cDNA was linearized with *Sph*I and transcribed using the large-scale T7 mMESSAGE mMACHINE transcription kit (Ambion). The plasmids pCI.neo containing the gene for Kv 1.3 were linearized with *Not*I (Promega) and transcribed like Kv 1.2. Stage-V and -VI *Xenopus laevis* oocytes were harvested by partial ovariectomy under anaesthesia (3-aminobenzoic acid ethyl ester methanesulfonate salt, 0.5 g/l, Sigma). Anaesthetized animals were kept on ice during dissection. The oocytes were defolliculated by treatment with 2 mg/ml collagenase (Sigma) in Ca^{2+}-free ND-96 solution (in mM: NaCl 96, KCl 2, $MgCl_2$ 1, HEPES 5 adjusted to pH 7.5). Between 1 and 24 h after defolliculation, oocytes were injected with 10 nl of 50–100 ng/μl cRNA. The oocytes were then incubated in ND-96 solution (supplemented with 50 mg/ml gentamycin sulphate) at 16 °C for one day.

1.8. Electrophysiological measurements

Two-electrode voltage-clamp recordings were performed at room temperature using a GeneClamp 500 amplifier (Axon Instruments) controlled by a pClamp data acquisition system (Axon Instruments). Whole-cell currents from oocytes were recorded 1 day after injection. Voltage and current electrodes were filled with 3 M KCl. Resistances of both electrodes were kept as low as possible (<0.5 MΩ). Bath solution composition was (in mM): NaCl 96, KCl 2, $CaCl_2$ 1.8, $MgCl_2$ 2 and HEPES 5 (pH 7.4). Using a four-pole low-pass Bessel filter, currents were filtered at 1 kHz and sampled at 2 kHz. Current traces were evoked in an oocyte expressing Kv channels by depolarizations to 0 mV from a holding potential of −90 mV. Statistical analysis between groups of data was carried out using the Student's *t*-test and a probability of <0.05 was considered to be statistically significant.

2. Results

2.1. Isolation and purification of κ-KTx1.3

Ultracentrifugation of *H. spinifer* resulted in a filtrate of Mr < 5000, which would likely contain the neurotoxins directed against K^+ channels. The venom ultrafiltrate was then directly subjected to reverse-phase HPLC which resulted in the separation of over 30 small peptides (Fig. 1A). The most prominent peak (identified by arrow) was subjected to mass spectrometry and found to contain a near-homogenous (~97% purity) peptide with a molecular mass of 2620.58 ± 0.55 Da (electrospray ionization mass spectrometry) (Fig. 1B) and 2620.71 Da (MALDI–TOF mass spectrometry) (data not shown). This peptide was subsequently identified as κ-KTx1.3.

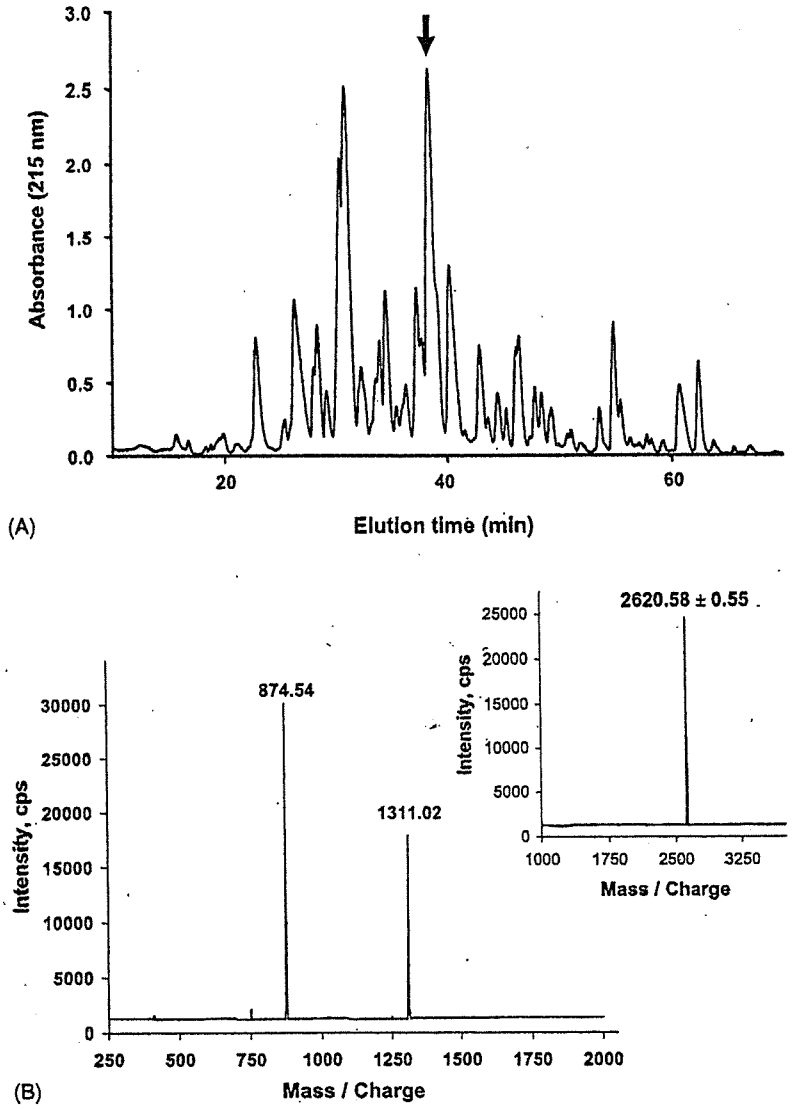

Fig. 1. Isolation and purification of κ-KTx1.3: (A) reverse-phase HPLC of *H. spinifer* venom ultrafiltrate (Mr < 5000) on a Sephasil C8 (0.21 cm × 10 cm) column equilibrated with 0.1% trifluoroacetic acid. Proteins were eluted with a linear gradient (20–50% over 80 min) of eluent (80% acetonitrile in 0.1% trifluoroacetic acid) at a flow rate of 1 ml/min. The elution of proteins was monitored at 215 nm. The peak indicated by arrow was identified as κ-KTx1.3 and subjected to mass spectroscopy, (B) electrospray ionization mass spectrum of κ-KTx1.3 shows a series of multiply charged ions, corresponding to a single, homogenous peptide of molecular mass 2620.58 ± 0.55 Da (inset, reconstructed spectrum).

2.2. *Determination of the amino acid sequence of κ-KTx1.3*

We were able to unequivocally identify all the residues and determine the complete amino acid sequence of both native (blank cycles where cysteine residues are found) and pyridylethylated κ-KTx1.3. κ-KTx1.3 has 23 amino acid residues including four cysteine residues. Its calculated mass, with the expected two disulfide bridges, was 2620.91, which coincides well with the estimated molecular mass. It shared ~60% identity to κ-hefutoxin 1 (κ-KTx1.1) and κ-hefutoxin 2 (κ-KTx1.2) [13] and almost no sequence similarity to any other known scorpion toxins. Hence, κ-KTx1.3 was identified as the third member of the recently identified κ-KTx subfamily of weak K^+ channel toxins and was designated as κ-KTx1.3 (Fig. 2). The amino acid sequence of κ-KTx1.3 is deposited in the SWISS-PROT protein database (accession number P83655).

2.3. *Solid phase synthesis of κ-KTx1.3*

Due to the low yield (~0.1%) of native κ-KTx1.3, it was chemically synthesized for further characterization. Since κ-hefutoxin 1 and κ-hefutoxin 2 had amidated and free-carboxy termini, respectively, linear precursors of κ-KTx1.3 with both, amidated and free carboxy-termini, were synthesized by Fmoc solid phase method. Random air oxidation of the linear precursors of κ-KTx1.3 afforded a major product which was purified until it migrated as a single peak on analytical HPLC. The purity of synthetic

κ-KTx 1.1	Hefutoxin-1	GHACYRNCWREGNDEETCKERC
κ-KTx 1.2	Hefutoxin-2	GHACYRNCWREGNDEETCKERCG
κ-KTx 1.3	Native	GFGCYRSCWKAGHDEETCKKECS
κ-KTx 1.3	K20E	GFGCYRSCWKAGHDEETCKEECS
κ-KTx 1.3	K20A	GFGCYRSCWKAGHDEETCKAECS
κ-KTx 1.3	K20R	GFGCYRSCWKAGHDEETCKRECS
κ-KTx 1.1	Hefutoxin-1 E20K R21E	GHACYRNCWREGNDEETCKKEC

4 8 18 22

Fig. 2. Amino acid sequences of the members of the κ-KTx subfamily. The cysteines are numbered and the disulfide linkages outlined. The residues contributing to the functional dyad are in bold. The residues by which κ-KTx1.3 differs from κ-hefutoxin 1 are shaded in grey and the mutated residues in κ-KTx1.3 and κ-hefutoxin 1 are underlined. The Swiss-Prot (Swiss Institute for Bioinformatics) accession numbers are P82852, P82851 and P83655, respectively, for κ-hefutoxin 1 and 2 (*Heterometrus fulvipes*) and κ-KTx1.3 (*Heterometrus spinifer*). The International Union of Pure and Applied Chemistry one-letter notation for amino acids is used (*J Biol Chem* 1968;243:3557–9).

peptides was confirmed by analytical HPLC and MALDI–TOF mass spectrometry. Synthetic κ-KTx1.3 with either amidated or free carboxy-termini were co-injected with native κ-KTx1.3 on to an analytical HPLC which resulted in κ-KTx1.3 (OH), but not κ-KTx1.3 (NH_2), eluting together with the native peptide as a single peak (Fig. 3). This confirmed that κ-KTx1.3 has a free carboxyl group at its carboxy-terminal end.

2.4. Assignment of disulfide pairings in κ-KTx1.3

To determine the disulfide bond pairings, synthetic κ-KTx1.3 was digested with trypsin which yielded three digest products of MW 1639.60, 1511.53 and 1039.08 that agreed with the calculated MW for the digested fragments SCWKAGHDEETCKK + H_2O, SCWKAGHDEETCK + H_2O and GFGCYRECS + H_2O, respectively (Fig. 4). These data confirmed that κ-KTx1.3, like κ-hefutoxin-1 and 2 [13], also has disulfide combinations of C1–C4 and C2–C3 (Fig. 5A and 5B). The circular dichroism spectra of synthetic κ-KTx1.3 (OH) revealed that it has a conformation typical of α-helical structure (data not shown).

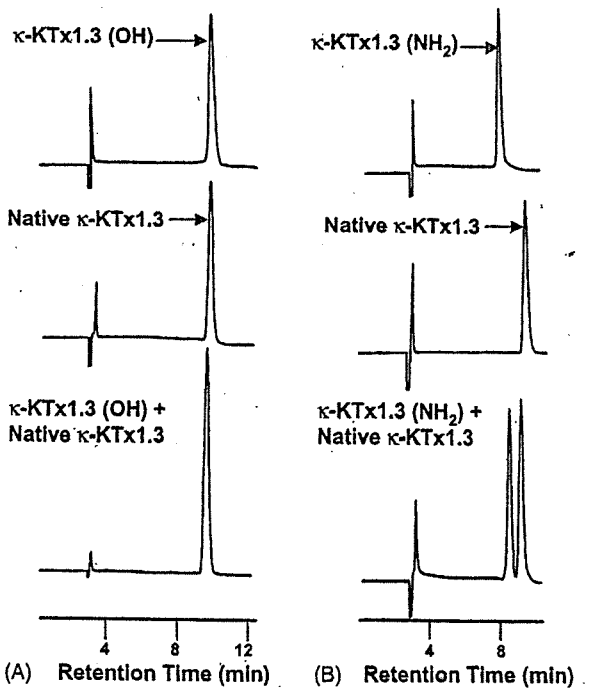

Fig. 3. Synthesis of κ-KTx1.3. Linear precursors of κ-KTx1.3 with free (κ-KTx1.3(OH)) and amidated (κ-KTx1.3(NH_2)) carboxy termini were synthesized by solid phase methodology with Fmoc chemistry. Synthetic κ-KTx1.3(OH) and κ-KTx1.3(NH_2) were co-injected with native κ-KTx1.3 on to an analytical HPLC which resulted in κ-KTx1.3 (OH) (A), but not κ-KTx1.3 (NH_2) (B), eluting together with the native peptide as a single peak. This confirmed that κ-KTx1.3 has a free carboxyl group at its carboxy-terminal end.

2.5. Molecular modeling of κ-KTx1.3

Since κ-KTx1.3 shared ~60% identity in primary sequence including disulfide pairing with κ-hefutoxin 1, the NMR structure of the latter (PDB accession number 1HP9) was used as a template to create a molecular model of κ-KTx1.3. Like κ-hefutoxin 1, the model of κ-KTx1.3 revealed a compact structure consisting of two parallel α-helices that are held together by the two disulfide bridges (C4–C22 and C8–C18) (Fig. 5A and 5B). The K^+ channel blocking activity of κ-hefutoxin was deduced based on the presence of the minimum functional dyad, K19 and Y5, positioned at a distance of ~6.01 Å between the α-carbon of the lysine and the center of the aromatic face of the tyrosine (Fig. 5C) [13]. The model of κ-KTx1.3 also

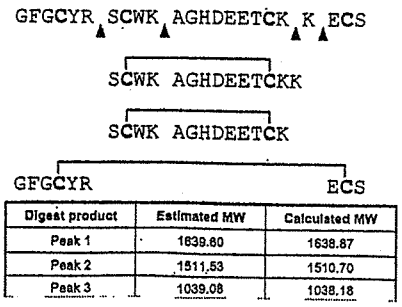

Digest product	Estimated MW	Calculated MW
Peak 1	1639.60	1638.87
Peak 2	1511.53	1510.70
Peak 3	1039.08	1038.18

Fig. 4. Assignment of disulfide pairings in κ-KTx1.3. To determine the disulfide bond pairings, synthetic κ-KTx1.3 was digested with trypsin which yielded three digest products of MW 1639.60, 1511.53 and 1039.08 that agreed with the calculated MW for the digested fragments SCWKAGHDEETCKK + H_2O, SCWKAGHDEETCK + H_2O and GFGCYRECS + H_2O, respectively. These data confirmed that κ-KTx1.3 has disulfide combinations of C1–C4 and C2–C3.

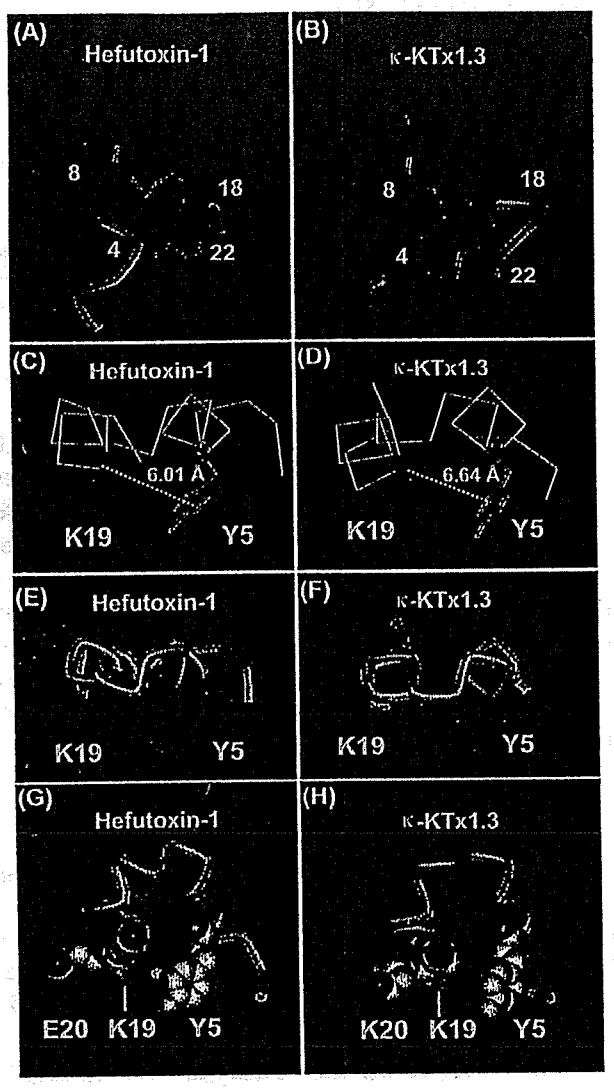

Fig. 5. Molecular model of κ-KTx 1.3. The NMR structure of κ-hefutoxin 1 (A) (PDB accession number 1HP9; first out of the ensemble of 20 lowest energy structures) was used as a template to construct a molecular model of κ-KTX1.3 (B) using InsightII (Molecular Simulations Inc., USA). Like κ-hefutoxin 1, the model of κ-KTx1.3 revealed a compact structure consisting of two parallel α-helices that are held together by the two disulfide bridges (C4–C22 and C8–C18) (shown in green). The K^+ blocking activity of κ-hefutoxin 1 was deduced based on the presence of the functional dyad, Y5 and K19, positioned at a distance of 6.01 Å between the α-carbon of the lysine and the center of the aromatic face of the tyrosine (C). The molecular model of κ-KTX1.3 also showed the presence of this dyad (Y5, K19) positioned at a distance of 6.64 Å (D). The α-carbon backbone structure is presented in C and D. In both, κ-hefutoxin 1 (E) and κ-KTX1.3 (F), the dyad residues (shown in Corey–Pauling–Koltun presentation) K19 (violet) and Y5 (green) protrude out of a flat surface formed by the edges of the two parallel α-helices, in conformity with the general architecture of other pore-blocking K^+ channel toxins. The amino acid residue at position 20, Glu20 in κ-hefutoxin 1 (G) and Lys20 in κ-KTX1.3 (H) is also shown in relation to the functional dyad (K19, Y5) in the respective toxins. In (G) and (H), both toxins are shown in similar orientations along the long-axis of the side chain of K19 with the selected residues in Corey–Pauling–Koltun representation. The amino acid residues are coloured according to their charge, with blue and red depicting positive and negative charge, respectively. (For interpretation of the references to colour in this figure legend, the reader is referred to the web version of the article.)

revealed the presence of this functional dyad (K19/Y5) which were positioned at a comparable distance of 6.64 Å between them (Fig. 5D). As observed in κ-hefutoxin 1 (Fig. 5E), both K19 and Y5 in κ-KTx1.3 also protrude out of a flat surface formed by the edges of the two parallel α-helices (Fig. 5F). These data strongly suggested that the molecular targets of κ-KTx1.3 could also be voltage-gated K^+ channels.

2.6. Biological activity of κ-KTx1.3

Synthetic κ-KTx1.3 was screened for K^+ channel blocking activity in *X. laevis* oocytes expressing a single type of voltage-gated K^+ channel (Kv 1.1, Kv 1.2 or Kv 1.3). κ-KTx1.3 did not inhibit currents through Kv 1.1, Kv 1.2 or Kv 1.3 channels even at high concentrations of 1 mM (see Fig. 6) suggesting that it was functionally inert on Kv 1 channels.

2.7. Rationale for the synthesis of mutants of κ-KTx1.3

On analyzing the primary sequences of κ-KTx1.3 and κ-hefutoxins 1 and 2, it was found that the functional dyad lysine (K19) in κ-KTx1.3 was flanked by another lysine (K20) (Figs. 2 and 5). Experimental and modeling data have previously shown the dyad lysine to be a key player in binding to K^+ channels principally via electrostatic interactions between its positively charged extremity and carbonyl oxygen atoms of the channel selectivity filter [9,10,19]. It was thus hypothesized that the presence of an additional positive charge in a position adjacent to the putative dyad lysine (Fig. 5) could impair the electrostatic interactions necessary for toxin binding. Thus, mutants of κ-KTx1.3, with the lysine at position 20 mutated to a neutral (κ-KTx1.3 K20A) or another positively charged (κ-KTx1.3 K20R) amino acid or subjected to charge-reversal (κ-KTx1.3 K20E), were chemically synthesized for further electrophysiological characterization.

2.8. Functional characterization of κ-KTx1.3 mutants

The effects of the κ-KTx1.3 mutants on oocyte-expressed Kv 1.1, Kv 1.2 or Kv 1.3 channels were studied. The application of 200 μM of κ-KTx1.3 K20E produced 80.3 and 38.2% blockade of Kv 1.2 and Kv 1.3 channels, respectively, whereas only a small effect (10.7% blockade) was observed on Kv 1.1 channels (Fig. 6). The addition of 200 μM κ-KTx1.3 K20A resulted in a 44.6% blockade of Kv 1.1 channels as well as 35.0 and 44.1% blockade of Kv 1.2 and Kv 1.3 channels, respectively (Fig. 6). κ-KTx1.3 K20R did not produce any blockade of the three Kv 1 channels.

The blockade induced by κ-KTx1.3 K20A on Kv 1.1, Kv 1.2 and Kv 1.3 (Fig. 7A–C), and by κ-KTx1.3 K20E on Kv 1.2 and Kv 1.3 (Fig. 7D and 7E), were concentration-dependent. The IC_{50} values for κ-KTx1.3 K20A deter-

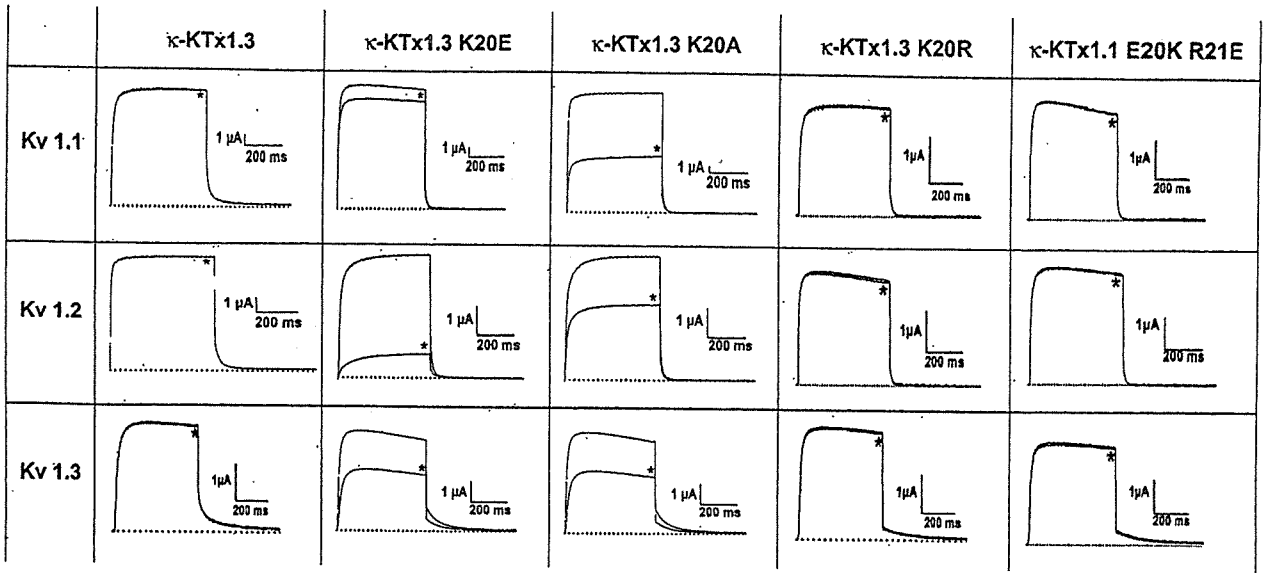

Fig. 6. Effects of κ-KTx1.3, κ-KTx1.3 K20E, κ-KTx1.3 K20A, κ-KTx1.3 K20R and the double mutant κ-KTx1.1 E20K R21E on Kv 1.1, Kv 1.2 and Kv 1.3 channels expressed in *X. laevis* oocytes. Current traces were evoked in oocytes expressing Kv channels by depolarizations to 0 mV from a holding potential of −90 mV and then clamped back to −50 mV. Asterisk (*) indicates the comparison of control condition to the presence of the toxin. After application of 200 μM of κ-KTx1.3 K20E, a small effect was observed on Kv 1.1 channels (10.7 ± 2.4% block) whereas 80.3 ± 6.9% and 38.2 ± 4.1% blockade were obtained on Kv 1.2 and Kv 1.3 channels, respectively. After application of 200 μM of κ-KTx1.3 K20A, we observed 44.6 ± 3.1% block on Kv 1.1 channels, 35.0 ± 3.8% on Kv 1.2 channels and 44.1 ± 4.2% block on Kv 1.3 channels. Native κ-KTx1.3 as well as κ-KTx1.3 K20R and κ-KTx1.1 E20K R21E did not produce any block of the Kv 1 channels tested. Data are the mean ± S.E.M. of at least four experiments.

mined by a sigmoidal fit were 110.7 ± 7.7 μM for Kv 1.1, 36.9 ± 4.9 μM for Kv 1.2 and 115.7 ± 7.3 μM for Kv 1.3 (Fig. 6F). The IC_{50} values for κ-KTx1.3 K20E were 36.8 ± 4.9 μM for Kv 1.2 and 53.7 ± 6.7 μM for Kv 1.3 (Fig. 6F). The block by both mutants was reversible upon washing-out and also shown to be voltage-independent (data not shown).

3. Discussion

Molecular models based on comparative analysis of the protein or peptide under investigation can pave the way for key experimental work to determine their biological activity more rapidly and in greater detail [20]. In this context, the significant structural homology between κ-KTx1.3 and κ-hefutoxin 1, including the presence of the functional dyad residues Y5 and K19 in identical positions, strongly suggested that the biological activity of κ-KTx1.3 would correspond to that of κ-hefutoxin 1. Previously, it was on the basis of the secondary structure of κ-hefutoxin 1, specifically the presence of the functional dyad (Y5, K19), that its K^+ channel blocking activity was predicted [13]. This was experimentally confirmed by the demonstration that κ-hefutoxin 1 produced concentration-dependent, voltage-independent and reversible blockade of currents through oocyte-expressed Kv 1.2 and Kv 1.3 channels with IC_{50} values of 40 and 150 μM, respectively [13]. Kv 1.1 channels were not significantly affected by κ-hefutoxin, suggesting that its affinity for Kv 1-type channels was Kv 1.2 > Kv 1.3 ⋙ Kv 1.1. Furthermore, mutational analysis identified Y5 and K19 as the key residues for bioactivity since their mutation to alanine, singly or together, resulted in a total loss of K^+ channel blockade [13].

Despite their unrelated structures and sources, toxins derived from animal venoms across different phyla, contain a key "dyad" composed of a positively charged residue (usually a lysine) and a hydrophobic residue (usually an aromatic amino acid) that constitute a minimal functional core for these toxins to bind to Kv 1 channels [8,13–15,21–23]. Additional residues may confer each toxin with a specific binding profile, the determination of subtype specificity for instance [21,24]. Interestingly, recent studies have also suggested that the functional dyad per se is not a prerequisite for toxin binding to Kv channels, in which case, other residues may act to form "multipoint interactions" with these channels [25–27].

This diverse array of toxins, however, all bind to a highly conserved region among K+ channels located at the pore helix and selectivity filter [9,10,15,22,27]. Generally, the binding of toxins to Kv 1 channels involves a combination of electrostatic, hydrophobic and hydrogen bonding interactions [27]. The major determinant of toxin binding to Kv 1 channels is likely to be the electrostatic interactions between the extremity of the dyad lysine, which protrudes into the ion-channel pore, and carbonyl oxygen atoms of residues from the highly conserved region of the channel selectivity filter [9,10,15,19,22,27,28]. Hydrophobic interactions between the dyad hydrophobic residue and aromatic residues protruding in the channel vestibule are believed to reinforce the critical electrostatic interaction

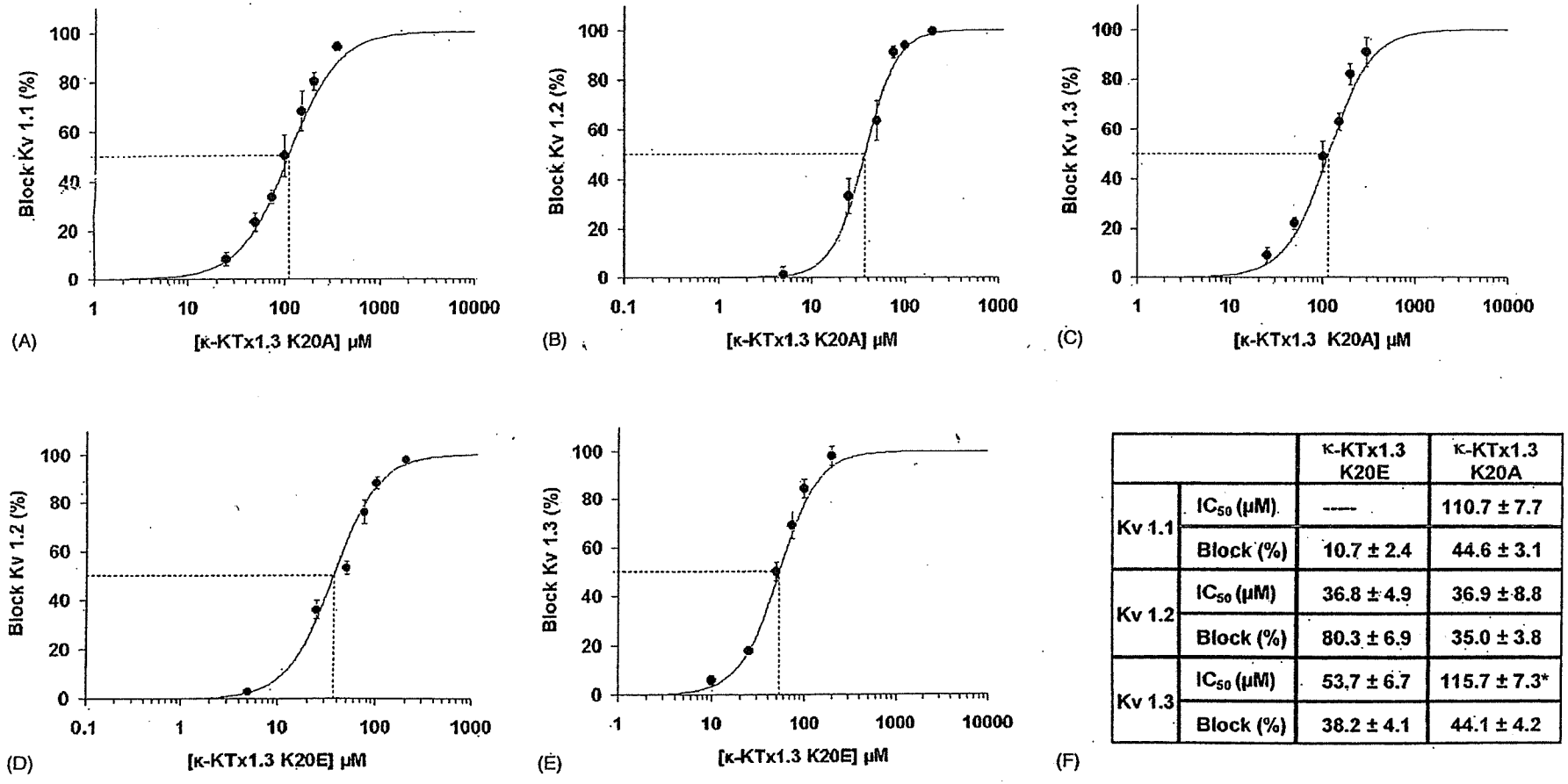

(F)

		κ-KTx1.3 K20E	κ-KTx1.3 K20A
Kv 1.1	IC_{50} (μM)	-----	110.7 ± 7.7
	Block (%)	10.7 ± 2.4	44.6 ± 3.1
Kv 1.2	IC_{50} (μM)	36.8 ± 4.9	36.9 ± 8.8
	Block (%)	80.3 ± 6.9	35.0 ± 3.8
Kv 1.3	IC_{50} (μM)	53.7 ± 6.7	115.7 ± 7.3*
	Block (%)	38.2 ± 4.1	44.1 ± 4.2

Fig. 7. Concentration dependence of the block induced by κ-KTx1.3 K20A on Kv 1.1, Kv 1.2 and Kv 1.3 (A–C) and κ-KTx1.3 K20E on Kv 1.2 and Kv 1.3 (D and E) channels. Currents were normalized as a function of the maximal block percentage set at 100%. Currents were evoked by a depolarization to 0 mV from a holding potential of −90 mV. The IC_{50} values and the maximal percentage block are shown (F). Data are the mean ± S.E.M. of at least four experiments at each concentration. $^{*}p < 0.05$, statistically significant when compared to κ-KTx1.3K20E.

by surrounding the lysine side-chain and allowing its exclusion from solvent [22]. Thus, it appears that the conserved functional dyad residues from scorpion toxins bind via conserved molecular interactions to Kv 1 channels.

However, on screening κ-KTx1.3 for K^+ channel blocking activity on oocyte-expressed Kv 1-type channels, it was found that the toxin did not show the expected electrophysiological effects even at concentrations as high as 1 mM. On analyzing the primary structure of κ-KTx1.3, it was hypothesized that the presence of an additional positively charged residue (K20) that was found flanking the putative key lysine (K19) in its primary sequence could hinder the proposed electrostatic interaction of κ-KTx1.3 with the K^+ channel. Interestingly, the single mutation of K20 in κ-KTx1.3 to a negatively charged glutamic acid, as found in κ-hefutoxin 1, resulted in the mutant κ-KTx1.3 K20E acquiring biological activity almost identical to that of κ-hefutoxin 1 with respect to subtype selectivity and affinity. Accordingly, κ-KTx1.3 K20E produced blockade of Kv 1.2 (IC_{50} ~37 μM) and Kv 1.3 (IC_{50} ~54 μM) but not Kv 1.1 channels. In contrast, the mutant κ-KTx1.3 K20A produced blockade of both Kv 1.2 (IC_{50} ~37 μM) and Kv 1.3 (IC_{50} ~116 μM) and in addition, also acquired affinity for Kv 1.1 channels (IC_{50} ~111 μM). Although, both κ-hefutoxin 1 and the κ-KTx1.3 mutants produced partial blockade of Kv 1 channels, such partial blocks of these channels have also been reported before for several scorpion toxins, possibly due to imperfect ion channel pore occlusion [28–30]. To provide conclusive evidence of our hypothesis, two other mutants were synthesized: κ-KTx1.3 K20R, wherein lysine 20 was mutated to arginine, and κ-KTx1.1 E20K R21E, a double mutant of κ-hefutoxin 1, with the residues at positions 20 and 21 mutated to lysine and glutamic acid, respectively, as found in κ-KTx1.3. Both caused no significant block on the three Kv channels.

These data suggest that the presence of an additional positive charge in a position adjacent to the dyad lysine in κ-KTx1.3 is sufficient, presumably by electrostatic repulsion, to prevent its ability to produce functional blockade of Kv 1.2 and Kv 1.3 channels. On the other hand, the functional blockade of Kv 1.1 channels by κ-KTx1.3 was impeded if the dyad lysine was flanked by either a positively or negatively charged amino acid. Together, these data support previous reports [13–15,22–24] that Kv 1 channel toxins establish high affinity interactions principally or in part via electrostatic interactions involving the key dyad lysine and in addition suggest that the toxin-induced functional blockade of Kv 1 channels may be easily compromised by changes in the charge environment of the dyad region.

While the κ-KTx subfamily of scorpion toxins, which interact only weakly with Kv 1 channel subtypes, are yet to be investigated for biological activity against other K^+ channels, it must also be remembered that despite the remarkable achievements made in the recent past with respect to the biology of K^+ channels, many K^+ channel currents remain elusive and await the discovery of novel ligands for their identification and characterization [10,12]. Hence it is possible that scorpion toxins such as κ-hefutoxin 1 and κ-KTx1.3 may have been selected by natural evolution for other high-affinity molecular targets that are still currently unknown.

Acknowledgements

K.S. was supported by a grant-in-aid from the Ministry of Education, Science, Sports, Culture and Technology of Japan. S.N. was the recipient of a research scholarship from the National University of Singapore.

References

[1] Gwee MCE, Nirthanan S, Khoo HE, Gopalakrishnakone P, Kini RM, Cheah LS. Autonomic effects of some scorpion venoms and toxins. Clin Exp Pharmacol Physiol 2002;29:795–801.
[2] Martin-Euclaire M-F. Neurotoxins from scorpion venoms. In: Massaro EJ, editor. Handbook of neurotoxicology, vol. 1. Totowa, NJ: Humana; 2001. p. 503–8.
[3] Olamendi-Portugal T, Gomez-Lagunas F, Gurrola GB, Possani LD. A novel structural class of K^+ channel blocking toxin from the scorpion *Pandinus imperator*. Biochem J 1996;315:977–81.
[4] Kharrat R, Mansuelle P, Sampieri F, Crest M, Oughideni R, Van Rietschoten J. Maurotoxin, a four disulfide bridge toxin from *Scorpio maurus* venom: purification, structure and action on potassium channels. FEBS Lett 1997;406:284–90.
[5] Lebrun B, Romi-Lebrun R, Martin-Eauclaire MF, Yasuda A, Ishiguro M, Oyama Y, et al. A four-disulphide toxin, with high affinity towards voltage-gated K+ channels, isolated from *Heterometrus spinifer* (Scorpionidae) venom. Biochem J 1997;328:321–7.
[6] Strong PN. Potassium channel toxins. Pharmacol Ther 1990;46:137–62.
[7] Possani LD, Merino E, Corona M, Becerril B. Scorpion genes and peptides specific for potassium channels: structure, function and evolution. In: Menez A, editor. Perspectives in molecular toxinology. Chichester, England: John Wiley & Sons; 2002. p. 201–11.
[8] Darbon H, Blanc E, Sabatier J-M. Three-dimensional structure of scorpion toxins: towards a new model of interaction with potassium channels. Perspect Drug Discov Des 1999;15/16:41–60.
[9] Garcia ML, Gao Y, McManus OB, Kaczorowski GJ. Potassium channels: from scorpion venoms to high-resolution structure. Toxicon 2001;39:739–48.
[10] Rodriguez de la Vega RC, Merino E, Becerril B, Possani LD. Novel interactions between K^+ channels and scorpion toxins. Trends Pharmacol Sci 2003;24:222–7.
[11] Tytgat J, Chandy KG, Garcia ML, Gutman GA, Martin-Euclaire M-F, Walt JJ, et al. A unified nomenclature for short-chain peptides isolated from scorpion venoms: α-KTx molecular subfamilies. Trends Pharmacol Sci 1999;20:444–7.
[12] Possani LD, Selisko B, Gurrola GB. Structure and function of scorpion toxins affecting K+-channels. Perspect Drug Discov Des 1999;15/16:15–40.
[13] Srinivasan KN, Sivaraja V, Huys I, Sasaki T, Cheng B, Kumar TKS, et al. κ-Hefutoxin 1, a novel toxin from *Heterometrus fulvipes* with unique structure and function. Importance of the functional dyad in potassium channel selectivity. J Biol Chem 2002;277:30040–7.
[14] Dauplais M, Lecoq A, Song J, Cotton J, Jamin N, Gilquin B, et al. On the convergent evolution of animal toxins. Conservation of a dyad of functional residues in potassium channel-blocking toxins with unrelated structures. J Biol Chem 1997;272:4302–9.

[15] Menez A, Servent D, Gasparini S. The binding sites of animal toxins involve two components: a clue for selectivity, evolution and design of proteins? In: Menez A, editor. Perspectives in molecular toxinology. Chichester, England: John Wiley & Sons; 2002. p. 175–200.
[16] Nirthanan S, Joseph JS, Gopalakrishnakone P, Khoo HE, Cheah LS, Gwee MC... Biochemical and pharmacological characterization of the venom of the black scorpion (*Heterometrus spinifer*). Biochem Pharmacol 2002;63:49–55.
[17] Srinivasan KN, Nirthanan S, Sasaki T, Sato K, Cheng B, Gwee MCE, et al. Functional site of bukatoxin, a K-type sodium channel neurotoxin from the Chinese scorpion (*Buthus Martensi* Karsch) venom: probable role of the 52 PDKVP 56 loop. FEBS Lett 2001;494:145–9.
[18] Liman ER, Tytgat J, Hess P. Subunit stoichiometry of a mammalian K^+ channel determined by construction of multimeric cDNAs. Neuron 1992;9:861–71.
[19] Miller C. The charybdotoxin family of K^+ channel-blocking peptides. Neuron 1995;15:5–10.
[20] Possani LD, Rodriguez de la Vega RC. Response to Xu et al.: Hypothesis-driven science paves the way for new discoveries. Trends Pharmacol Sci 2003;24:448–9.
[21] Gasparini S, Danse J-M, Lecoq A, Pinkasfeld S, Zinn-Justin S, Young LC, et al. Delineation of the functional site of α-dendrotoxin. The functional topographies of dendrotoxins are different but share a conserved core with those of other Kv 1 potassium channel-blocking toxins. J Biol Chem 1998;273:25393–403.
[22] Gilquin B, Racape J, Wrisch A, Visan V, Lecoq A, Grissmer S, et al. Structure of the BgK-Kv 1.1 complex based on distance restraints identified by double mutant cycles. Molecular basis for convergent evolution of Kv 1 channel blockers. J Biol Chem 2002;277:37406–13.
[23] Huys I, Tytgat J. Evidence for a function-specific mutation in the neurotoxin, parabutoxin 3. Eur J Neurosci 2003;17:1786–92.
[24] Alessandri-Haber N, Lecoq A, Gasparini S, Grangier-Macmath G, Jacquet G, Harvey AL, et al. Mapping the functional anatomy of BgK on Kv 1.1, Kv 1. 2 and Kv 1. 3. Clues to design analogs with enhanced selectivity. J Biol Chem 1999;274:35653–61.
[25] Batista CV, Gomez-Lagunas F, Rodriguez de la Vega RC, Hajdu P, Panyi G, Gaspar R, et al. Two novel toxins from the Amazonian scorpion *Tityus cambridgei* that block Kv 1.3 and *Shaker* B K^+ channels with distinctly different affinities. Biochem Biophys Acta 2002;1601:123–31.
[26] Mouhat S, Mosbah A, Visan V, Wulff H, Delepierre M, Darbon H, et al. The "functional" dyad of scorpion toxin Pi1 is not itself a prerequisite for toxin binding to the voltage-gated Kv 1.2 potassium channels. Biochem J 2004;377:25–36.
[27] Xu C-Q, Zhu S-Y, Chi C-W, Tytgat J. Turret and pore block of K^+ channels: what is the difference?. Trends Pharmacol Sci 2003;24: 446–68.
[28] M'Barek S, Mosbah A, Sandoz G, Fajloun Z, Olamendi-Portugal T, Rochat H, et al. Synthesis and characterization of Pi4, a scorpion toxin from *Pandinus imperator* that acts on K^+ channels. Eur J Biochem 2003;270:3583–92.
[29] Fajloun Z, Carlier E, Lecomte C, Geib S, Di Luccio E, Bichet D, et al. Chemical synthesis and characterization of Pi1, a scorpion toxin from *Pandinus imperator* active on K^+ channels. Eur J Biochem 2000;267:5149–55.
[30] Huys I, Dyason K, Waelkens E, Verdonck F, van Zyl J, du Plessis J, et al. Purification, characterization and biosynthesis of parabutoxin 3, a component of *Parabuthus transvaalicus* venom. Eur J Biochem 2002;269:1854–65.

J|A|C|S
ARTICLES
Published on Web 06/29/2005

Selective Zinc Sensor Molecules with Various Affinities for Zn^{2+}, Revealing Dynamics and Regional Distribution of Synaptically Released Zn^{2+} in Hippocampal Slices

Kensuke Komatsu,† Kazuya Kikuchi,*,†,‡ Hirotatsu Kojima,† Yasuteru Urano,†,‡ and Tetsuo Nagano*,†

Contribution from the Graduate School of Pharmaceutical Sciences, The University of Tokyo, 7-3-1 Hongo, Bunkyo-ku, Tokyo 113-0033, Japan, and Presto, JST Agency, Honcho, Kawaguchi-shi, Saitama 332-0012, Japan

Received January 17, 2005; E-mail: tlong@mol.f.u-tokyo.ac.jp; kkikuchi@mol.f.u-tokyo.ac.jp

Abstract: We have developed a series of fluorescent Zn^{2+} sensor molecules with distinct affinities for Zn^{2+}, because biological Zn^{2+} concentrations vary over a wide range from sub-nanomolar to millimolar. The new sensors have K_d values in the range of 10^{-8}–10^{-4} M, compared with 2.7 nM for ZnAF-2. They do not fluoresce in the presence of other biologically important metal ions such as calcium or magnesium, and they can detect Zn^{2+} within 100 ms. In cultured cells, the fluorescence intensity of ZnAF-2 was saturated at low Zn^{2+} concentration, while that of ZnAF-3 (K_d = 0.79 μM) was not saturated even at relatively high Zn^{2+} concentrations. In hippocampal slices, we measured synaptic release of Zn^{2+} in response to high-potassium-induced depolarization. ZnAF-2 showed similar levels of fluorescence increase in dentate gyrus (DG), CA3 and CA1, which were indistinguishable. However, ZnAF-3 showed a fluorescence increase only in DG. Thus, by using a combination of sensor molecules, it was demonstrated for the first time that a higher Zn^{2+} concentration is released in DG than in CA3 or CA1 and that we can easily visualize Zn^{2+} concentration over a wide range. We believe that the use of various combinations of ZnAF family members will offer unprecedented versatility for fluorescence-microscopic imaging of Zn^{2+} in biological applications.

Introduction

For over a century, zinc (Zn^{2+}) has been known as an essential trace element, acting as a structural component of proteins or in the catalytic site of enzymes.[1] In general, Zn^{2+} is tightly associated with proteins and peptides. However, recent advances in cell biology have revealed a fraction of Zn^{2+} that is free or chelatable in some organs (brain,[2] pancreas,[3] and spermatozoa[4]). In the brain, a considerable amount of chelatable Zn^{2+} is sequestered in the vesicles of presynaptic neurons and is released when the neurons are active.[5] Zn^{2+} is also associated with neuronal disorders,[6] though its role in them is poorly understood. So there is much interest in its detection in vivo, where its concentration varies from 10^{-10} M in the cytoplasm[7] to 10^{-4} M in some vesicles.[8] However, the lack of appropriate detecting tools, especially for such a broad concentration range, hinders further investigation of this spectroscopically silent metal ion.

Fluorescent sensor molecules offer useful information about chelatable Zn^{2+} in cellular systems, because we can study the concentration or distribution of Zn^{2+} in real time,[9] and fluorescence imaging of Zn^{2+} has become a widely and frequently used technique. The first reported sensor molecules for cellular Zn^{2+} were arenesulfonamides of 8-aminoquinoline, such as TSQ [10] and Zinquin.[11] They form 1:2 complexes with Zn^{2+}, emitting strong fluorescence on UV excitation. Since then, various kinds of fluorescent Zn^{2+} sensor molecules have been developed and examined, such as TSQ derivatives,[12] peptide or protein-based sensors,[13] sensors for ratiometric measurement,[14] and others.[15] Above all, various fluorescein derivatives were introduced: NGs,[16] ZPs,[17] FluoZins,[18] ZnAFs,[19] and others.[20] Fluorescein derivatives have many advantages over

† The University of Tokyo.
‡ JST Agency.

(1) (a) Vallee, B. L.; Falchuk, K. H. *Physiol. Rev.* **1993**, *73*, 79–118. (b) Berg, J. M.; Shi, Y. G. *Science* **1996**, *271*, 1081–1085.
(2) (a) Frederickson, C. J. *Int. Rev. Neurobiol.* **1989**, *31*, 145–238. (b) Frederickson, C. J.; Bush, A. I. *Biometals* **2001**, *14*, 353–366. (c) Li, Y.; Hough, C.; Sarvey, J. *Sci. STKE* **2003**, *182*, 19.
(3) (a) Zalewski, P. D.; Millard, S. H.; Forbes, I. J.; Kapaniris, O.; Slavotinek, A.; Betts, W. H.; Ward, A. D.; Lincoln, S. F.; Mahadevan, I. *J. Histochem. Cytochem.* **1994**, *42*, 877–884. (b) Qian, W. J.; Gee, K. R.; Kennedy, R. T. *Anal. Chem.* **2003**, *75*, 3468–3475.
(4) Zalewski, P. D.; Jian, X.; Soon, L. L. L.; Breed, W. G.; Seamark, R. F.; Lincoln, S. F.; Ward, A. D.; Sun, F. Z. *Reprod., Fertil. Dev.* **1996**, *8*, 1097–1105.
(5) (a) Assaf, S. Y.; Chung, S. H. *Nature* **1984**, *308*, 734–736. (b) Howell, G. A.; Welch, M. G.; Frederickson, C. J. *Nature* **1984**, *308*, 736–738.
(6) Bush, A. I. *Curr. Opin. Chem. Biol.* **2000**, *4*, 184–191.
(7) (a) Canzoniero, L. M. T.; Sensi, S. L.; Choi, D. W. *Neurobiol. Dis.* **1997**, *4*, 275–279. (b) Outten, C. E.; O'Halloran, T. V. *Science* **2001**, *292*, 2488–2492. (c) Thompson, R. B.; Peterson, D.; Mahoney, W.; Cramer, M.; Maliwal, B. P.; Suh, S. W.; Frederickson, C.; Fierke, C.; Herman, P. *J. Neurosci. Methods* **2002**, *118*, 63–75. (d) Finney, L. A.; O'Halloran, T. V. *Science* **2003**, *300*, 931–936.
(8) Frederickson, C. J.; Klitenick, M. A.; Manton, W. I.; Kirkpatrick, J. B. *Brain Res.* **1983**, *273*, 335–339.
(9) Mason, W. T. *Fluorescent and Luminescent Probes for Biological Activity*; 2nd ed.; Academic Press: New York, 1999.
(10) Frederickson, C. J.; Kasarskis, E. J.; Ringo, D.; Frederickson, R. E. *J. Neurosci. Methods* **1987**, *20*, 91–103.
(11) Zalewski, P. D.; Forbes, I. J.; Betts, W. H. *Biochem. J.* **1993**, *296*, 403–408.

10.1021/ja050301e CCC: $30.25

Zinquin. The high quantum yield in aqueous solution provides high sensitivity in the cellular environment, and the excitation wavelength in the visible range minimizes cell damage during irradiation. These sensors have led to great advances in Zn^{2+} biology, and further development of sensor molecules would be very valuable.[21]

We set out several criteria for developing novel fluorescent Zn^{2+} sensor molecules. First, for intensity-based measurement, the sensor should have no signal in the absence of Zn^{2+}, and the signal should increase in the presence of Zn^{2+} in an all-or-none fashion. Second, the sensor should be selective for Zn^{2+}, without interference by biologically important metal ions, such as Ca^{2+} or Mg^{2+}. Third, complexation and decomplexation with Zn^{2+} should be rapid, to provide a fast response. Fourth, for intracellular study, the sensor should be derivatizable into a cell-permeable form that can penetrate through the cell membrane and be hydrolyzed intracellularly to afford the sensor, which is then trapped in the cell. Fifth, their affinity for Zn^{2+} should be appropriate for the Zn^{2+} concentration range of interest.

We previously showed that ZnAFs, which satisfy most of the requirements mentioned above, can serve as useful tools for biological applications.[19,22] However, the affinity for Zn^{2+} remains an issue. To follow changes of Zn^{2+} concentration, it is desirable to use a sensor molecule whose apparent dissociation constant (K_d) is near the target concentration of Zn^{2+}. Almost all Zn^{2+} sensor molecules recently developed have K_d values in the nanomolar region (ZnAF-2, 2.7 nM), because cytosolic free Zn^{2+} concentration is controlled at ~1 nM or lower.[7] Neither Zn^{2+} deficiency nor Zn^{2+} excess affects cell viability and function,[23] and these sensors can easily be used in cytoplasm, etc. However, at higher concentrations of Zn^{2+}, the fluorescence intensity of these sensors would be saturated. Zn^{2+} is known to be sequestered in synaptic vesicles of many excitatory forebrain neurons, and the concentration of Zn^{2+} inside the vesicle was reported to be in the micro- to millimolar range.[8] This vesicular Zn^{2+} is also released into synaptic space, where it is estimated to achieve peak levels of 10−30 μM.[24] In such circumstances, sensor molecules with high affinity would have no ability to detect changes of Zn^{2+} concentration. So, for precise analysis of the biological roles of Zn^{2+}, we require a range of sensor molecules with K_d values not only in the nM range, but also higher.

Among Zn^{2+} sensor molecules so far reported, only Newport Green ($K_d \sim 1$ μM) has been used as a low-affinity Zn^{2+} sensor to detect synaptically released Zn^{2+}, for which purpose the Zn^{2+} concentration was calculated on the basis of the K_d value.[24] There is little other evidence to support the idea that the release of Zn^{2+} reaches micromolar levels, so confirmation remains desirable.

Our purpose in this study is to develop a range of low-affinity sensor molecules whose K_d values are higher than nanomolar order without any loss of favorable characteristics, such as low basal fluorescence and selectivity for Zn^{2+}.

In designing low-affinity sensor molecules, we chose ZnAF-2 as a basal structure. ZnAF-2 has a fluorescein fluorophore conjugated to *N*,*N*-bis(2-pyridylmethyl)ethylenediamine as a Zn^{2+} chelator. The design of the chelator was based on the structure of TPEN (*N*,*N*,*N*′,*N*′-tetrakis(2-pyridylmethyl)ethylenediamine). These groups offer the following advantages. Derivatives of fluorescein that are amino-substituted at the benzoic acid moiety emit little fluorescence due to the photo-induced electron transfer (PeT) quenching pathway, resulting in low basal fluorescence and high sensitivity.[20a] TPEN is known as a selective chelator of Zn^{2+} over Ca^{2+} or Mg^{2+}.[25] For intracellular application, a cell-permeant form can be obtained readily, because the TPEN moiety itself cannot be protonated at physiological pH, so the sensor remains intact. Moreover, the structural separation of sensor and chelator moieties means that modification of the chelator should not affect the fluorescence properties, such as maximum/minimum quantum yield or excitation/emission wavelength. This approach, leaving the fluorophore intact, is a characteristic advantage of fluorescent sensors utilizing the PeT mechanism. Therefore, we set out to develop a series of Zn^{2+} sensor molecules by modification of

(12) (a) Budde, T.; Minta, A.; White, J. A.; Kay, A. R. *Neuroscience* **1997**, *79*, 347−358. (b) Nasir, M. S.; Fahrni, C. J.; Suhy, D. A.; Kolodsick, K. J.; Singer, C. P.; O'Halloran, T. V. *J. Biol. Inorg. Chem.* **1999**, *4*, 775−783. (c) Fahrni, C. J.; O'Halloran, T. V. *J. Am. Chem. Soc.* **1999**, *121*, 11448−11458. (d) Kimber, M. C.; Mahadevan, I. B.; Lincoln, S. F.; Ward, A. D.; Betts, W. H. *Aust. J. Chem.* **2001**, *54*, 43−49. (e) Pearce, D. A.; Jotterand, N.; Carrico, I. S.; Imperiali, B. *J. Am. Chem. Soc.* **2001**, *123*, 5160−5161. (f) Hendrickson, K. M.; Geue, J. P.; Wyness, O.; Lincoln, S. F.; Ward, A. D. *J. Am. Chem. Soc.* **2003**, *125*, 3889−3895.

(13) (a) Walkup, G. K.; Imperiali, B. *J. Am. Chem. Soc.* **1996**, *118*, 3053−3054. (b) Walkup, G. K.; Imperiali, B. *J. Am. Chem. Soc.* **1997**, *119*, 3443−3450. (c) Walkup, G. K.; Imperiali, B. *J. Org. Chem.* **1998**, *63*, 6727−6731. (d) Thompson, R. B.; Maliwal, B. P.; Fierke, C. A. *Anal. Chem.* **1998**, *70*, 1749−1754. (e) Barondeau, D. P.; Kassmann, C. J.; Tainer, J. A.; Getzoff, E. D. *J. Am. Chem. Soc.* **2002**, *124*, 3522−3524. (f) Hong, S. H.; Maret, W. *Proc. Natl. Acad. Sci. U.S.A.* **2003**, *100*, 2255−2260. (g) Shults, M. D.; Pearce, D. A.; Imperiali, B. *J. Am. Chem. Soc.* **2003**, *125*, 10591−10597.

(14) (a) Maruyama, S.; Kikuchi, K.; Hirano, T.; Urano, Y.; Nagano, T. *J. Am. Chem. Soc.* **2002**, *124*, 10650−10651. (b) Henary, M. M.; Fahrni, C. J. *J. Phys. Chem. A* **2002**, *106*, 5210−5220. (c) Taki, M.; Wolford, J. L.; O'Halloran, T. V. *J. Am. Chem. Soc.* **2004**, *126*, 712−713. (d) Henary, M. M.; Wu, Y. G.; Fahrni, C. I. *Che.−Eur. J.* **2004**, *10*, 3015−3025.

(15) (a) Hanaoka, K.; Kikuchi, K.; Kojima, H.; Urano, Y.; Nagano, T. *Angew. Chem., Int. Ed.* **2003**, *42*, 2996−2999. (b) Hanaoka, K.; Kikuchi, K.; Kojima, H.; Urano, Y.; Nagano, T. *J. Am. Chem. Soc.* **2004**, *126*, 12470−12476. (c) Lim, N. C.; Yao, L.; Freake, H. C.; Bruckner, C. *Bioorg. Med. Chem. Lett.* **2003**, *13*, 2251−2254. (d) Koutaka, H.; Kosuge, J.; Fukasaku, N.; Hirano, T.; Kikuchi, K.; Urano, Y.; Kojima, H.; Nagano, T. *Chem. Pharm. Bull.* **2004**, *52*, 700−703.

(16) Haugland, R. P. *Handbook of Fluorescent Probes and Research Products*; 8th ed.; Molecular Probes, Inc.: Eugene, OR, 2001.

(17) (a) Walkup, G. K.; Burdette, S. C.; Lippard, S. J.; Tsien, R. Y. *J. Am. Chem. Soc.* **2000**, *122*, 5644−5645. (b) Burdette, S. C.; Walkup, G. K.; Spingler, B.; Tsien, R. Y.; Lippard, S. J. *J. Am. Chem. Soc.* **2001**, *123*, 7831−7841. (c) Burdette, S. C.; Frederickson, C. J.; Bu, W. M.; Lippard, S. J. *J. Am. Chem. Soc.* **2003**, *125*, 1778−1787. (d) Nolan, E. M.; Burdette, S. C.; Harvey, J. H.; Hilderbrand, S. A.; Lippard, S. J. *Inorg. Chem.* **2004**, *43*, 2624−2635. (e) Chang, C. J.; Nolan, E. M.; Jaworski, J.; Burdette, S. C.; Sheng, M.; Lippard, S. J. *Chem. Biol.* **2004**, *11*, 203−210. (f) Chang, C. J.; Nolan, E. M.; Jaworski, J.; Okamoto, K. I.; Hayashi, Y.; Sheng, M.; Lippard, S. J. *Inorg. Chem.* **2004**, *43*, 6774−6779.

(18) (a) Gee, K. R.; Zhou, Z. L.; Ton-That, D.; Sensi, S. L.; Weiss, J. H. *Cell Calcium* **2002**, *31*, 245−251. (b)Gee, K. R.; Zhou, Z. L.; Qian, W. J.; Kennedy, R. *J. Am. Chem. Soc.* **2002**, *124*, 776−778.

(19) (a) Hirano, T.; Kikuchi, K.; Urano, Y.; Higuchi, T.; Nagano, T. *J. Am. Chem. Soc.* **2000**, *122*, 12399−12400. (b) Hirano, T.; Kikuchi, K.; Urano, Y.; Nagano, T. *J. Am. Chem. Soc.* **2002**, *124*, 6555−6562.

(20) (a) Hirano, T.; Kikuchi, K.; Urano, Y.; Higuchi, T.; Nagano, T. *Angew. Chem.-Int. Edit.* **2000**, *39*, 1052−1054. (b) Sensi, S. L.; Ton-That, D.; Weiss, J. H.; Rothe, A.; Gee, K. R. *Cell Calcium* **2003**, *34*, 281−284. (c) Chang, C. J.; Jaworski, J.; Nolan, E. M.; Sheng, M.; Lippard, S. J. *Proc. Natl. Acad. Sci. U.S.A.* **2004**, *101*, 1129−1134.

(21) (a) Frederickson, C. *Sci. STKE* **2003**, *182*, 18. (b) Jiang, P. J.; Guo, Z. J. *Coord. Chem. Rev.* **2004**, *248*, 205−229. (c) Kikuchi, K.; Komatsu, K.; Nagano, T. *Curr. Opin. Chem. Biol.* **2004**, *8*, 182−191.

(22) Ueno, S.; Tsukamoto, M.; Hirano, T.; Kikuchi, K.; Yamada, M. K.; Nishiyama, N.; Nagano, T.; Matsuki, N.; Ikegaya, Y. *J. Cell Biol.* **2002**, *158*, 215−220.

(23) (a) MacDiarmid, C. W.; Milanick, M. A.; Eide, D. J. *J. Biol. Chem.* **2003**, *278*, 15065−15072. (b) Colvin, R. A.; Fontaine, C. P.; Laskowski, M.; Thomas, D. *Eur. J. Pharmacol.* **2003**, *479*, 171−185.

(24) (a) Li, Y.; Hough, C. J.; Suh, S. W.; Sarvey, J. M.; Frederickson, C. J. *J. Neurophysiol.* **2001**, *86*, 2597−2604. (b) Li, Y.; Hough, C. J.; Frederickson, C. J.; Sarvey, J. M. *J. Neurosci.* **2001**, *21*, 8015−8025.

(25) Arslan, P.; Divirgilio, F.; Beltrame, M.; Tsien, R. Y.; Pozzan, T. *J. Biol. Chem.* **1985**, *260*, 2719−2727.

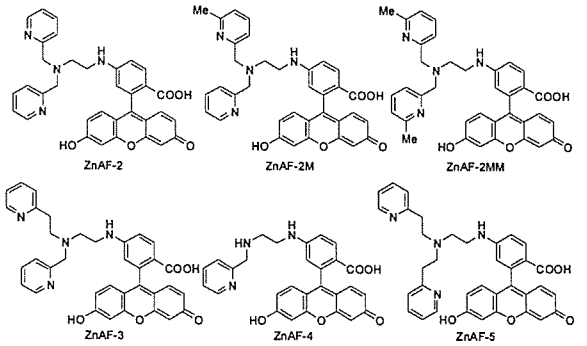

Figure 1. Structures of ZnAF family members. ZnAF-2 was previously reported to visualize Zn^{2+} in brain slices. The other sensor molecules were newly synthesized.

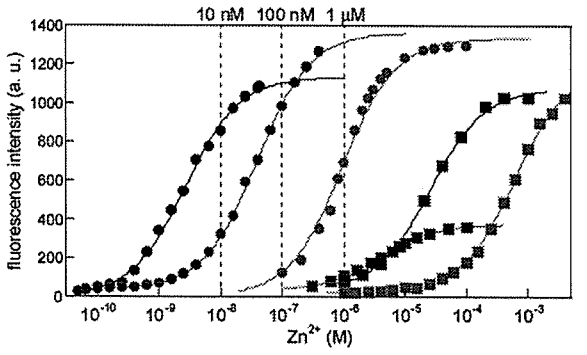

Figure 2. Changes of fluorescence intensity for 1 μM ZnAFs (ZnAF-2, black circle; ZnAF-2M, red circle; ZnAF-2MM, red square; ZnAF-3, blue circle; ZnAF-4, black square; and ZnAF-5, blue square) as a function of the concentration of free Zn^{2+} in 100 mM HEPES buffer (pH 7.4, $I = 0.1$ ($NaNO_3$)).

the TPEN moiety to obtain various K_d values without affecting the selectivity against other ions.

Here, we report a series of fluorescent sensor molecules for Zn^{2+} with various K_d values from nanomolar up to millimolar range. Their design, synthesis, and fluorescence properties are described. We also present applications to cultured cells and hippocampal slices.

Results and Discussion

Design and Synthesis. Figure 1 illustrates the structures of Zn^{2+} sensor molecules, ZnAF-2 and its new derivatives. ZnAF-2 was synthesized by conjugating 5-aminofluorescein and dipicolylamine via a linker, dibromoethane, so we introduced various chelators instead of dipicolylamine and left the fluorophore unchanged. The design was based on three strategies. First, we introduced steric hindrance at the nitrogen atom on the pyridine ring by substituting a methyl group at the 6-position (ZnAF-2M, ZnAF-2MM). Second, we removed one ligand, picolylamine (ZnAF-4). Last, we increased the distance between the ligands (ZnAF-3, ZnAF-5). The synthetic schemes for these sensors are described in the Supporting Information.

Fluorescence Properties. We measured the fluorescence intensity of these sensor molecules in various concentrations of Zn^{2+}. As we had expected, these sensors showed changes in fluorescence intensity at higher Zn^{2+} concentrations than ZnAF-2 (Figure 2) but retained almost the same fluorescence properties, such as absorption/emission wavelength and maximum/minimum quantum yield, which is convenient when using and comparing several sensors (Table 1). In each case, the fluorescence increase fitted well with a 1:1 binding model and the Hill coefficient of 1 suggests that a 1:1 Zn^{2+}–ZnAF complex was formed. The apparent dissociation constants were as follows: ZnAF-2M, 38 nM; ZnAF-2MM, 3.9 μM; ZnAF-3, 0.79 μM; ZnAF-4, 25 μM; and ZnAF-5, 0.60 mM (Table 2). Thus, we can follow a wide Zn^{2+} concentration range from 10^{-10} M up to 10^{-3} M by using different sensor molecules. Furthermore, by using them in combination, we can easily estimate the Zn^{2+} concentration. For example, if the concentration of free Zn^{2+} is 10 nM, there is strong fluorescence in ZnAF-2, weak fluorescence in ZnAF-2M, and no fluorescence in ZnAF-3 (Figure 2). At 100 nM Zn^{2+}, there is strong fluorescence in both ZnAF-2 and ZnAF-2M and little or no fluorescence in ZnAF-3. At 1 μM Zn^{2+}, there is strong fluorescence in ZnAF-3 and no fluorescence in ZnAF-4.

Among these sensors, ZnAF-2MM has lower quantum yield and fluorescence intensity in the presence of Zn^{2+} than the others. The fluorescence enhancement of ZnAFs, we consider, is attained through Zn^{2+} coordination to the amine on the benzoic acid moiety of fluorescein. In the absence of Zn^{2+}, the fluorescence is quenched due to the PeT from the benzoic acid moiety to the xanthene moiety. However, Zn^{2+} coordination alters the HOMO energy level of the benzoic acid moiety, thereby preventing PeT and leading to the enhancement of fluorescence from the xanthene moiety (fluorophore).[26] In ZnAF-2MM, the two methyl groups may alter the coordination structure of the Zn^{2+}–ZnAF complex, in a way that less strongly affects the HOMO energy level of the benzoic acid moiety, resulting in weak fluorescence.

Thus, we have completed developing a range of Zn^{2+} sensor molecules with various affinities for Zn^{2+} but whose fluorescence properties resemble those of ZnAF-2.

Determination of Complexing Rate. We then measured the complexing rate of these sensor molecules (Figure 3). When an excess amount of Zn^{2+} was added, all the sensors synthesized showed very rapid saturation of the fluorescence signal within about 100 ms, except for ZnAF-2MM, which reached maximum fluorescence after 1 s. Therefore, these sensors except for ZnAF-2MM are suitable for detecting rapid change in cellular Zn^{2+} concentration. The calculated association (k_{on}) and dissociation (k_{off}) constants are shown in Table 2. The k_{on} values of ZnAF-2M, ZnAF-3, and ZnAF-4 are almost the same as that of ZnAF-2, and the k_{off} values are larger than that of ZnAF-2, implying that these sensors can detect Zn^{2+} increase as fast as ZnAF-2 and Zn^{2+} decrease faster than ZnAF-2. ZnAF-2MM and ZnAF-5 have smaller k_{on} values than ZnAF-2. Apparently, just one picolyl group is important for the sensor to make a rapid complex with Zn^{2+}. On the other hand, the k_{off} values of ZnAFs are strongly dependent on the Zn^{2+} chelating structure. The k_{off} values of higher affinity sensors, such as ZnAF-2 or ZnAF-2M, may be relatively small but are not too slow for reversible assay of Zn^{2+} concentration. It is also clear that low-affinity sensors are more suitable for monitoring Zn^{2+} in a reversible fashion because of their large k_{off} values.

Metal Ion Selectivity. Figure 4 illustrates the fluorescence intensity of ZnAFs in the presence of various metal ions. Like

(26) Miura, T.; Urano, Y.; Tanaka, K.; Nagano, T.; Ohkubo, K.; Fukuzumi, S. *J. Am. Chem. Soc.* **2003**, *125*, 8666–8671.

Table 1. Absorbance and Fluorescence Properties of ZnAFs at pH 7.4[a]

	free			+Zn^{2+}		
Dye	λ_{max}	ϵ^b	Φ^c	λ_{max}	ϵ^b	Φ^c
ZnAF-2	490	7.8×10^4	0.023	492	7.6×10^4	0.3 2
ZnAF-2M	490	5.3×10^4	0.034	492	5.2×10^4	0.2 7
ZnAF-2MM	490	1.1×10^5	0.006	493	8.8×10^4	0.1 0
ZnAF-3	490	7.1×10^4	0.029	493	6.2×10^4	0.3 8
ZnAF-4	490	6.8×10^4	0.012	492	6.4×10^4	0.2 2
ZnAF-5	490	6.4×10^4	0.004	492	4.3×10^4	0.2 1

[a] All data were measured in 100 mM HEPES buffer (pH 7.4, $I = 0.1$ ($NaNO_3$)). [b] ϵ stands for extinction coefficient (M^{-1} cm^{-1}) measured at each λ_{max}. [c] Φ stands for quantum yield of fluorescence, determined using that of fluorescein (0.85) in 0.1 M NaOH aq. as a standard.

Table 2. Apparent Dissociation Constants (K_d) and Association and Dissociation Rate Constants (k_{on} and k_{off}) of ZnAFs in 100 mM HEPES Buffer (pH 7.4, $I = 0.1$ ($NaNO_3$)) at 25 °C

dye	K_d (M)	k_{on} ($M^{-1}s^{-1}$)	k_{off} (s^{-1})
ZnAF-2	2.7×10^{-9}	3.1×10^6	8.4×10^{-3}
ZnAF-2M	3.8×10^{-8}	1.3×10^6	4.9×10^{-2}
ZnAF-2MM	3.9×10^{-6}	6.9×10^4	0.28
ZnAF-3	7.9×10^{-7}	1.4×10^6	1.1
ZnAF-4	2.5×10^{-5}	1.6×10^6	51
ZnAF-5	6.0×10^{-4}	6.7×10^4	40

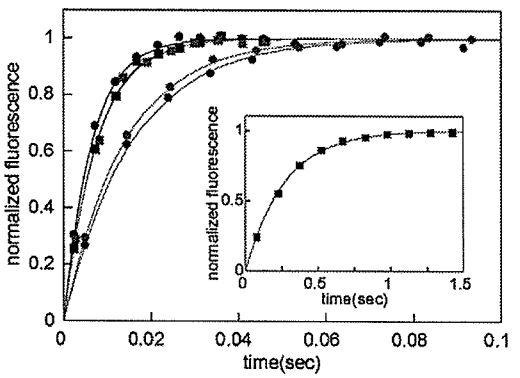

Figure 3. Time course measurement of the fluorescence intensity for 1 μM ZnAFs after mixing with Zn^{2+}. 50 μM Zn^{2+} was mixed with ZnAF-2 (black circle), ZnAF-2M (red circle), ZnAF-2MM (red square), and ZnAF-3 (blue circle). 1 mM Zn^{2+} was mixed with ZnAF-4 (black square) and ZnAF-5 (blue square). These data were measured in 100 mM HEPES buffer (pH 7.4, $I = 0.1$ ($NaNO_3$)) and 25 °C.

ZnAF-2, they show no response to biologically important metal ions, such as Ca^{2+} and Mg^{2+}, at millimolar concentration. Thus, the sensors with lower affinity for Zn^{2+} do not show reduced selectivity for Zn^{2+}. All the sensors have the same coordination atoms, and we think that this metal ion selectivity is mainly due to the character of nitrogen atom on the pyridine ring. In hard and soft acids and bases (HSAB) theory, pyridine is classified as a borderline base. It prefers Zn^{2+} to Ca^{2+} or Mg^{2+}, which is a hard acid. This preference would be important for the determination of the metal ion selectivity of ZnAFs. Some sensors show an increase in fluorescence intensity in the presence of some transition metals other than Zn^{2+}. Above all, Cd^{2+} shows a similar response to Zn^{2+}. However Cd^{2+} is rarely present in biological systems, so there would be no difficulty in biological applications.

Effect of pH. In addition to metal ion selectivity, it is important for many biological applications that the sensor does not respond to changes in pH. We measured the fluorescence intensity of ZnAFs at various pH values (Supporting Information, Figure S7). As in the case of ZnAF-2, the free bases of these sensors exhibit no significant emission enhancement upon acidification. Thus, the basal fluorescence intensity should be little affected by physiological pH changes.

Measuring Intracellular Zn^{2+}. We applied these sensor molecules to cultured cells or hippocampal slices. First, we measured the intracellular Zn^{2+} concentration of CHO cells to show their utility in fluorescence microscopic imaging by using membrane-permeable acetyl ester derivatives of ZnAF, ZnAF-2 DA,[19] and ZnAF-3 DA. These nonpolar compounds can easily penetrate through the cell membrane into the cytosol, where the acetyl groups are hydrolyzed by esterase to afford the Zn^{2+} sensors. After incubation with 10 μM sensors, cells showed weak fluorescence, suggesting that these sensors can be used intracellularly (data not shown). Then, we examined whether the difference of affinity is reflected in the fluorescence microscopic imaging of intracellular Zn^{2+} or not. The intracellular concentration of Zn^{2+} was controlled with a Zn^{2+} ionophore, pyrithione (2-mercaptopyridine *N*-oxide), which brings extracellular Zn^{2+} into the cytoplasm. We added various concentrations of Zn^{2+} with pyrithione, and the intracellular Zn^{2+} concentration was measured by fluorescence microscopy. Figure 5 shows the fluorescence response of each sensor molecule. With the increase of extracellular Zn^{2+} concentration from 0.3 to 300 μM, the fluorescence intensity of ZnAF-2 ($K_d = 2.7$ nM) was soon saturated. On the other hand, that of ZnAF-3 ($K_d = 0.79$ μM) was not saturated until 300 μM Zn^{2+}. This different response was clearly derived from the different affinity of the two sensors for Zn^{2+}. ZnAF-2 is superior for detecting lower Zn^{2+} concentrations, while ZnAF-3 can measure higher Zn^{2+} concentrations, which shows the importance of affinity for Zn^{2+} in cellular imaging. Thus, we can trace intracellular Zn^{2+} accurately by using combinations of several sensor molecules.

These results are in contrast with a previous report,[27] in which affinity for Zn^{2+} was suggested to be of less importance than dye concentration in fluorescence imaging; i.e., the dye concentration dominates the sensitivity of the reporting system. If the dye concentration is relatively high compared with the total ion pool available, the calibration of the dye signal to ion concentration may be affected, so care is necessary when using high intracellular dye concentrations. However, we consider that affinity is always an important factor in fluorescence imaging, as we have shown here. Using Zn^{2+} sensor molecules with suitable affinities should allow better calibration of the fluorescent signal to Zn^{2+} concentration.

(27) Dineley, K. E.; Malaiyandi, L. M.; Reynolds, I. J. *Mol. Pharmacol.* **2002**, *62*, 618−627.

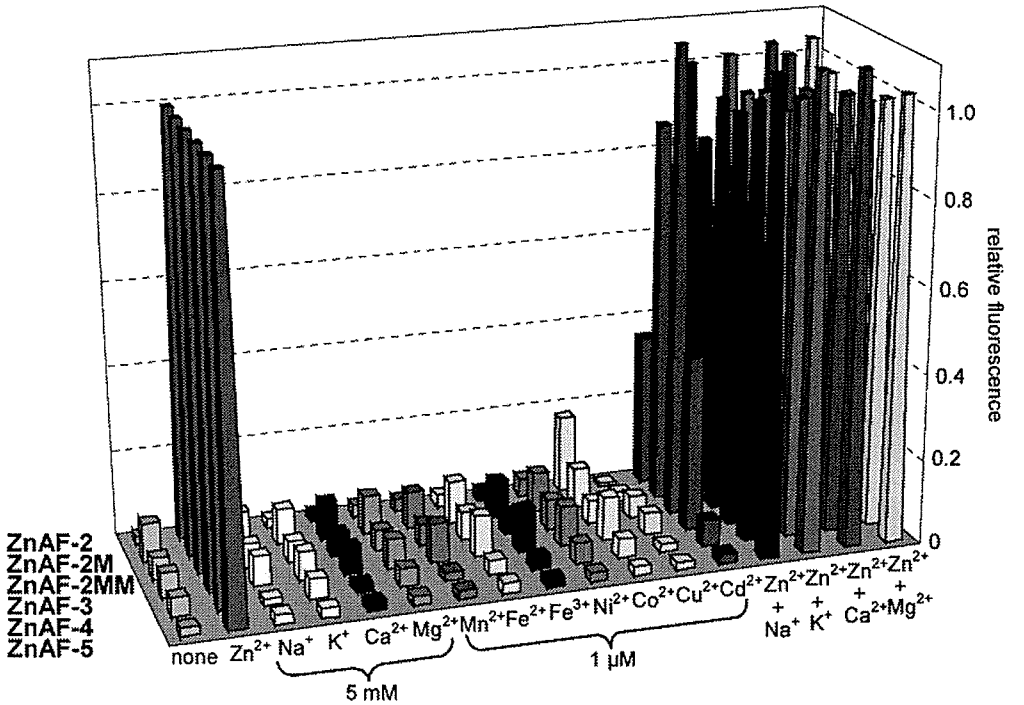

Figure 4. Relative fluorescence intensity of 1 μM ZnAFs in the presence of various metal ions. Na^+, K^+, Ca^{2+}, and Mg^{2+} were added at the concentration of 5 mM. Zn^{2+} was added at either 1 μM (ZnAF-2, ZnAF-2M) or 10 μM (ZnAF-2MM, ZnAF-3) or 100 μM (ZnAF-4, ZnAF-5). Other metals were added at 1 μM. These data were measured in 100 mM HEPES buffer (pH 7.4, I = 0.1 ($NaNO_3$)).

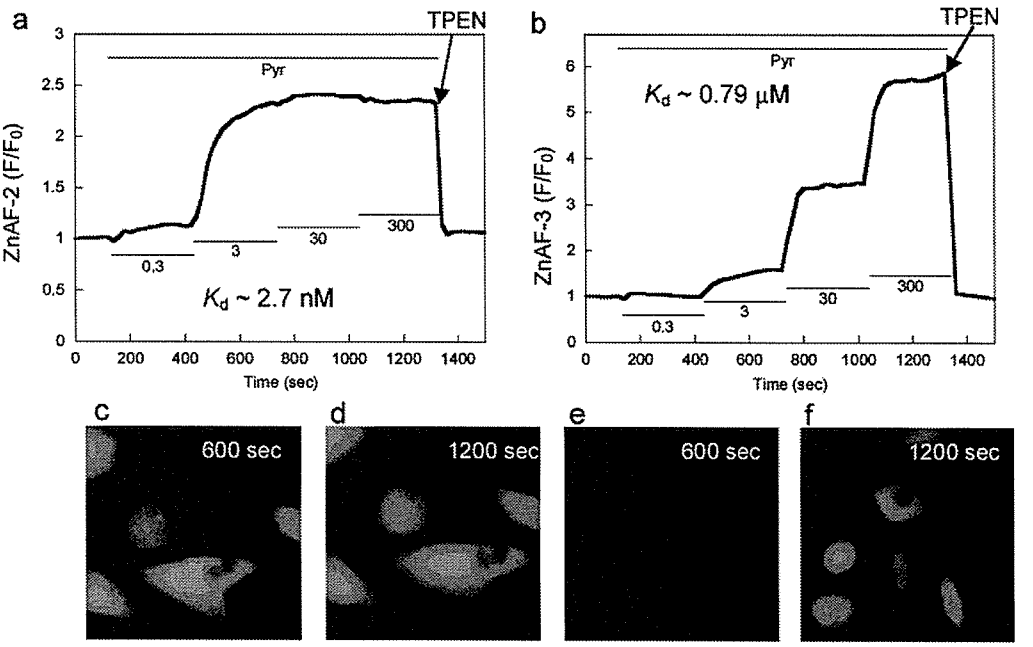

Figure 5. Fluorescence response of ZnAFs induced by intracellular Zn^{2+}. CHO cells incubated with 10 μM ZnAF-2 DA (a) or ZnAF-3 DA (b) for 30 min at room temperature were washed with PBS and fluorescence excited at 470−490 nm was measured at 20 s intervals. At 2 min, cells were exposed to pyrithione (Pyr, 100 μM) in the presence of sequentially increased concentrations of added extracellular Zn^{2+} (0.3, 3, 30, and 300 μM, each for 5 min) as indicated by the solid lines. Return of intracellular Zn^{2+} to the resting level was achieved by addition of TPEN (50 μM; starting at arrow). Fluorescence images incubated with ZnAF-2 DA (c, 600 s), (d, 1200 s), or ZnAF-3 DA (e, 600 s; f, 1200 s) are shown in the bottom panels.

Measuring Synaptically Released Zn^{2+}. For the analysis of Zn^{2+} in the central nervous system, we applied these sensors to hippocampal slices and measured synaptically released Zn^{2+} induced by membrane potential-depolarizing stimulation. All

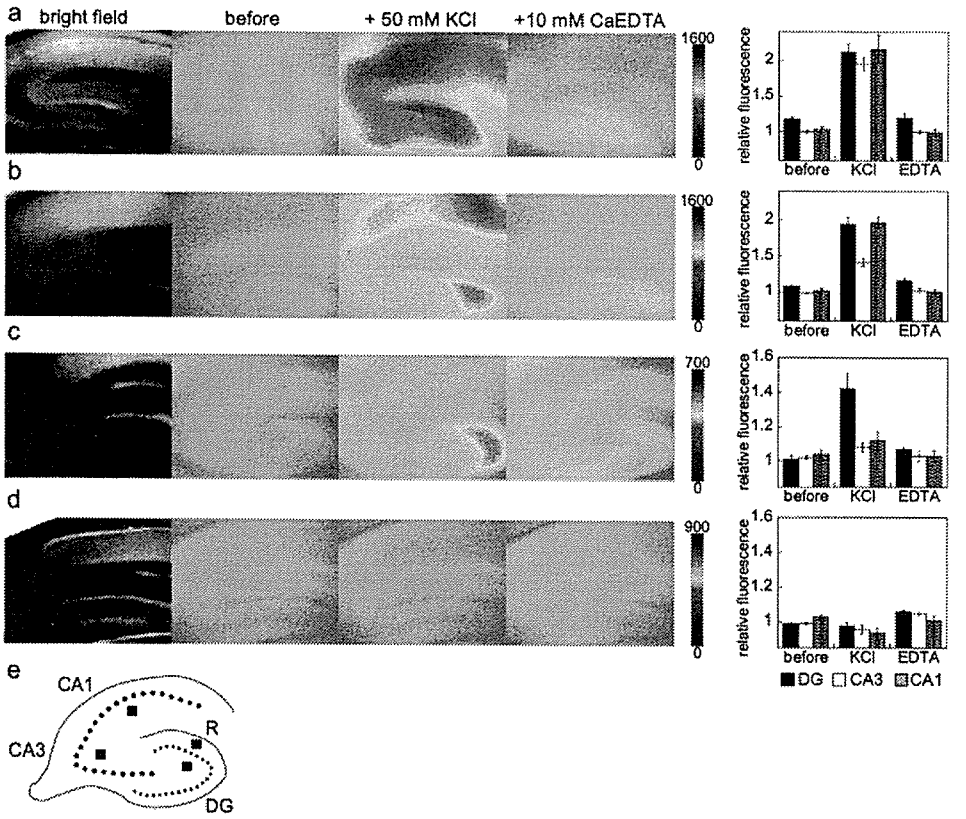

Figure 6. Fluorescence response of ZnAFs detecting extracellularly released Zn^{2+} in hippocampal slices. Fluorescence excited at 470−490 nm was measured soon after rat hippocampal slices were loaded with 1 μM ZnAF-2 (a), ZnAF-2M (b), ZnAF-3 (c), or ZnAF-4 (d). Then, 50 mM KCl (at 1 min) and 10 mM CaEDTA (at 10 min) were added to the imaging solution. Bright field images, fluorescence images at 0 min (before), at 3 min (+50 mM KCl), and at 15 min (+10 mM CaEDTA) are shown in each row. Relative fluorescence intensities of DG, CA3, and CA1 are shown in the bar graph, expressed as mean ± SE (n = 3 for ZnAF-2, ZnAF-3, and ZnAF-4 and n = 5 for ZnAF-2M). The bottom schematic (e) shows the approximate positions used for measurements of fluorescence intensity in the dentate gyrus (DG), CA3, CA1, and R (as a reference) region.

of the nerve terminals were stimulated into depolarization after addition of potassium ions. We observed a large fluorescence increase upon addition of 50 mM KCl to slices loaded with 1 μM ZnAF. To confirm that this fluorescence increase was due to an increase of extracellular Zn^{2+} concentration, we further added CaEDTA, an extracellular Zn^{2+} chelator. This treatment reduced the fluorescence intensity of ZnAF to the initial level, which confirmed that the indicator was responding to extracellular Zn^{2+} and that the extracellular Zn^{2+} concentration was below the detection level prior to depolarization. We acquired different fluorescence images after stimulation depending on the K_d value of the ZnAFs (Figure 6a−d). In the fluorescence imaging using ZnAF-2 (K_d = 2.7 nM), the fluorescence intensity increased mainly in three regions, the dentate gyrus (DG), CA3, and CA1, which were indistinguishable. Therefore, no regional difference of released Zn^{2+} concentration was observed using ZnAF-2, probably because of its high affinity for Zn^{2+}. With ZnAF-2M (K_d = 38 nM), on the other hand, the fluorescence intensity increased in DG and CA1, but increased less in CA3, and with ZnAF-3 (K_d = 0.79 μM), a fluorescence increase was seen only in DG. The lower affinity sensor, ZnAF-4 (K_d = 25 μM) showed no fluorescence increase. The mean increase of fluorescence intensity in each region is shown in the bar graph. So, these results demonstrate for the first time that a higher concentration of Zn^{2+} is released in DG than in CA3 or CA1, and a lower concentration of Zn^{2+} is released in CA3 than in DG or CA1.

A key advantage of using plural sensors is that estimation of the released Zn^{2+} concentration level is possible. In DG, there is a fluorescence response of ZnAF-3 (K_d = 0.79 μM) and no response of ZnAF-4 (K_d = 25 μM). Namely, the released Zn^{2+} concentration in DG is below the detection level for ZnAF-4. Thus, the released Zn^{2+} concentration is estimated to be of the order of 1 μM DG (Figure 2). Similarly, in both CA1 and CA3, there is a fluorescence response of ZnAF-2M (K_d = 38 nM) and no response of ZnAF-3. Thus, the released Zn^{2+} concentration level in CA1 and CA3 can be estimated to be of the order of 100 nM or less.

Thus, by using dyes with different affinity for Zn^{2+} for fluorescence imaging, we can obtain considerably more information from the same sample than would be possible with a single dye. Furthermore, it is clear that there is no single K_d value suitable for tracing all of the concentration levels of synaptically released Zn^{2+}, because a K_d value suitable for one region would give either no response or a saturated fluorescence signal in other regions. So, the importance of using several sensor molecules is clear, just as we had anticipated when designing this range of sensors. By virtue of having a spectrum

of affinities for Zn^{2+}, ZnAFs are the first Zn^{2+} sensor molecules not only to reveal regional differences but also to allow estimation of the concentrations of synaptically released Zn^{2+} in hippocampal slices. In addition, ZnAFs are also suitable for analyzing temporal changes of Zn^{2+}; a fast fluorescence increase and decrease in the CA1 region was visualized with ZnAF-2M (data not shown).

Previous reports indicate that electrical stimulation and potassium stimulation produce similar responses in terms of released Zn^{2+} concentration.[24] This would suggest that a similar concentration level of Zn^{2+} is released during natural neuronal activity. However, the reported concentration levels of released Zn^{2+} vary drastically. Li et al. suggested that synaptic release of Zn^{2+} during stimulation reaches micromolar levels.[24] They used the fluorescent sensor molecule Newport Green, which has an affinity of ~1 μM for Zn^{2+}. On the other hand, Kay examined synaptic release of Zn^{2+} using another fluorescent sensor molecule, FluoZin-3, whose K_d value is 15 nM and concluded that little Zn^{2+} (~6 nM) was released during stimulation.[28] Both estimations were done with a single sensor molecule, with quite different K_d values, and they utilized the maximum and minimum fluorescence intensity for Zn^{2+} calibration. However, our estimation is based on the use of several sensor molecules without relying on measurements of maximum or minimum fluorescence intensity. Moreover, our sensors have similar fluorescence properties, and only their affinity for Zn^{2+} differs. We think these features support the reliability of Zn^{2+} estimation with ZnAFs.

On the basis of the above results, our ZnAFs introduced here are expected to become useful tools in the investigation of Zn^{2+} biology, especially the role of Zn^{2+} in the central nervous system.[2d] These ZnAFs should have a wide range of application. In addition to synaptic release of Zn^{2+}, Zn^{2+} is suggested to be involved in excitotoxic neuronal death after head trauma, epilepsy, and cerebral ischemia and reperfusion.[29] Recently, extracellular accumulation of Zn^{2+} during ischemia and reperfusion was reported.[30] However, regional differences of Zn^{2+} over the areas of DG, CA3, and CA1 were not observed. Zn^{2+} sensor molecules with suitable K_d values may visualize regional differences, allowing detailed analysis of the Zn^{2+} distribution.

Although other Zn^{2+} sensor molecules with various affinities are available,[11g,13d] ZnAFs are the first sensor molecules suitable for both intra- and extracellular applications in biology. Combined with fluorescence microscopic imaging, ZnAFs have the potential to play a central role in the investigation of Zn^{2+} biology.

Conclusion

We have developed a range of fluorescent Zn^{2+} sensor molecules, ZnAF-2M, ZnAF-2MM, ZnAF-3, ZnAF-4, and ZnAF-5, whose K_d values range from nanomolar to subnanomolar levels. They all have similar fluorescence properties and differ only in their affinity for Zn^{2+}, without any loss of selectivity for Zn^{2+}. Using ZnAF-2 DA and ZnAF-3 DA, cell-permeable derivatives of ZnAFs, different responses to changes in intracellular Zn^{2+} concentration were observed. Extracellular Zn^{2+} release was also measured using ZnAFs and their use enabled us to detect regional difference in the Zn^{2+} release for the first time, as well as to estimate the approximate concentration of synaptically released Zn^{2+} in hippocampal slices. We can measure Zn^{2+} concentration over a wide range by using ZnAFs, which are expected to be useful probes for obtaining further insight into the physiological importance of Zn^{2+}.

Experimental Section

General Information. All reagents and solvents were of the highest commercial quality and were used without purification. ZnAF-2 and ZnAF-2 DA were purchased from Daiichi Pure Chemicals Co., Ltd. (Tokyo, Japan). ZnAF-2M, ZnAF-2MM, ZnAF-3, ZnAF-4, ZnAF-5, and ZnAF-3 DA were prepared as described in the Supporting Information. Dimethyl sulfoxide (DMSO), 2-[4-(2-hydroxyethyl)-1-piperazinyl]ethanesulfonic acid (HEPES), nitrilotriacetic acid (NTA), and *N*,*N*,*N*′,*N*′-tetrakis-(2-pyridylmethyl)ethylenediamine (TPEN) were purchased from Dojindo Laboratories, Ltd. (Kumamoto, Japan). All other reagents were purchased from either Tokyo Kasei Kogyo Co., Ltd. (Tokyo, Japan), or Wako Pure Chemical Industries, Ltd. (Osaka, Japan).

Fluorometric Analysis. Fluorescence spectroscopic studies were performed with a Hitachi F4500 (Tokyo, Japan). The slit width was 2.5 nm for both excitation and emission. The photomultiplier voltage was 750 V. ZnAFs were dissolved in DMSO to obtain 10 mM stock solutions. Fluorescence intensities of 1 μM ZnAFs as a function of free Zn^{2+} concentration were measured in 100 mM HEPES buffer (pH 7.4, $I = 0.1$ ($NaNO_3$)). Free Zn^{2+} concentration was controlled by using 0−9 mM $ZnSO_4$/10 mM NTA (nitrilotriacetic acid) systems[19a] for ZnAF-2 and ZnAF-2M and unbuffered Zn^{2+} for other ZnAFs. The fluorescence intensity data were fitted to eq 1, and K_d was calculated, where F is the fluorescence intensity, F_{max} is the maximum fluorescence intensity, F_0 is the fluorescence intensity with no addition of Zn^{2+}, and $[Zn^{2+}]_f$ is the free Zn^{2+} concentration.

$$F = F_0 + (F_{max} - F_0)([Zn^{2+}]_f)/(K_d + [Zn^{2+}]_f) \quad (1)$$

Relative quantum yields of fluorescence were obtained by comparing the area under the corrected emission spectrum of the sample at 492 nm with that of a solution of fluorescein in 0.1 M NaOH (quantum yield: 0.85). UV−visible spectra were measured with a Shimadzu UV-1600 (Tokyo, Japan).

Stopped-Flow Measurements. Stopped-flow experiments were performed with a SF-61 DX2 double-mixing stopped-flow spectrofluorimeter (Hi-Tech, Salisbury, U.K.) equipped with a monochromator between the 75 W xenon light source and the reaction cuvette excitation window. The quartz sample cuvette and syringes containing the reactants were maintained at 25 ± 0.1 °C by a circulating water bath. The pneumatic cylinder was driven by a nitrogen pressure of 6 bar, which resulted in an instrument dead time of 1 ms. A solution of 2 μM ZnAF in 100 mM HEPES buffer (pH 7.4, $I = 0.1$ ($NaNO_3$)) was combined with an equal volume of 100 μM or 2 mM of $ZnSO_4$. Fluorescence was measured with excitation at 492 nm and with emission at >530 nm, using a 530 cutoff filter. The fluorescence intensity data were fitted to eq 2, and k_{obs} was obtained, where F is the normalized fluorescence. Then, k_{on} and k_{off} were calculated as described previously.[19b]

$$F = 1 - \exp(-k_{obs}t) \quad (2)$$

Imaging System. The imaging system was comprised of an inverted fluorescence microscope (IX-71; Olympus, Tokyo, Japan), CoolSNAP HQ CCD camera (Roper Scientific, Tucson, AZ), and an image processor (MetaFluor; Universal Imaging Corp., Downingtown, PA). The microscope was equipped with a xenon lamp (AH2-RX; Olympus), an objective lens for CHO cells (PlanApo 60×/1.40 oil; Olympus) or

(28) Kay, A. R. *J. Neurosci.* **2003**, *23*, 6847−6855.
(29) (a) Choi, D. W.; Koh, J. Y. *Annu. Rev. Neurosci.* **1998**, *21*, 347−375. (b) Frederickson, C. J.; Hernandez, M. D.; McGinty, J. F. *Brain Res.* **1989**, *480*, 317−321. (c) Suh, S. W.; Chen, J. W.; Motamedi, M.; Bell, B.; Listiak, K.; Pons, N. F.; Danscher, G.; Frederickson, C. J. *Brain Res.* **2000**, *852*, 268−273.
(30) Wei, G.; Hough, C. J.; Li, Y.; Sarvey, J. M. *Neuroscience* **2004**, *125*, 867−877.

for hippocampal slices (UPlanAPo 4×/0.16; Olympus), an excitation filter (BP470-490; Olympus), a dichroic mirror (DM505; Olympus), and an emission filter (BA510-550; Olympus).

Preparation of Cells. CHO cells were cultured in Alpha medium (αMEM; Invitrogen Corp., Carlsbad, CA) containing 10% fetal bovine serum (Invitrogen Corp.), 1% penicillin (Invitrogen), and 1% streptomycin (Invitrogen) at 37 °C in a 5/95 CO_2/air incubator. Cells were passaged 3 days before dye loading on a 35 mm glass-based dish (Iwaki, Funabashi, Japan). Then the cells were rinsed with phosphate-buffered saline (PBS; Invitrogen), and incubated with PBS containing 10 μM ZnAF-2 DA or ZnAF-3 DA for 30 min at 37 °C. The cells were washed with PBS twice and mounted on the microscope stage. Fluorescence excited at 470−490 nm was measured at 20 s intervals, and the responses of three cells were compiled to generate a single trace.

Preparation of Rat Hippocampal Slices. The whole brains of adult Wistar rats (male, 200−250 g) were removed quickly under ether anesthesia and placed in ice-cold ACSF (artificial cerebrospinal fluid), which was aerated with 95/5 O_2/CO_2. The composition of ACSF was 124 mM NaCl, 2.5 mM KCl, 26 mM $NaHCO_3$, 1.25 mM NaH_2PO_4, 2.0 mM $CaCl_2$, 1.0 mM $MgCl_2$, and 10 mM glucose. The hippocampus was isolated, placed on an agar plate, and sliced into 300 μm thick slices with a rotary slicer (Model DTY 7700; Dosaka Co., Osaka, Japan). The fresh hippocampal slices were incubated in ACSF equilibrated with 95/5 O_2/CO_2 for more than 30 min at room temperature. Then each slice was transferred to a chamber on the microscope, where it was held in place by a metal wire ring with a stretched nylon net.

Acknowledgment. This work was supported in part by the Ministry of Education, Culture, Sports, Science and Technology of Japan (Grants for The Advanced and Innovational Research Program in Life Sciences to T.N., 15681012 and 16048206 to K.Kikuchi). K.Kikuchi was also supported by the Sankyo Foundation, by the Kanagawa Academy of Science, and by the Suzuken Memorial Foundation.

Supporting Information Available: Synthetic details and characterization of ZnAF-2M, ZnAF-2MM, ZnAF-3, ZnAF-4, ZnAF-5, and ZnAF-3 DA (PDF). This material is available free of charge via the Internet at http://pubs.acs.org.

JA050301E

THE JOURNAL OF BIOLOGICAL CHEMISTRY
Vol. 280, No. 22, Issue of June 3, pp. 21155–21161, 2005
Printed in U.S.A.

Inhibition of Autotaxin by Lysophosphatidic Acid and Sphingosine 1-Phosphate*[S]

Received for publication, November 22, 2004, and in revised form, February 18, 2005
Published, JBC Papers in Press, March 15, 2005, DOI 10.1074/jbc.M413183200

Laurens A. van Meeteren‡, Paula Ruurs‡, Evangelos Christodoulou§, James W. Goding¶, Hideo Takakusa‖, Kazuya Kikuchi‖, Anastassis Perrakis§, Tetsuo Nagano‖, and Wouter H. Moolenaar‡**

From the ‡Division of Cellular Biochemistry and Center for Biomedical Genetics and §Division of Molecular Carcinogenesis, The Netherlands Cancer Institute, Plesmanlaan 121, 1066 CX Amsterdam, The Netherlands, ¶Department of Pathology and Immunology, Monash Medical School, Alfred Hospital, Prahran 3181, Victoria, Australia, and ‖Graduate School of Pharmaceutical Sciences, University of Tokyo, Tokyo 113-0033, Japan

Autotaxin (ATX) or nucleotide pyrophosphatase/phosphodiesterase 2 (NPP2) is an NPP family member that promotes tumor cell motility, experimental metastasis, and angiogenesis. ATX primarily functions as a lysophospholipase D, generating the lipid mediator lysophosphatidic acid (LPA) from lysophosphatidylcholine. ATX uses a single catalytic site for the hydrolysis of both lipid and non-lipid phosphodiesters, but its regulation is not well understood. Using a new fluorescence resonance energy transfer-based phosphodiesterase sensor that reports ATX activity with high sensitivity, we show here that ATX is potently and specifically inhibited by LPA and sphingosine 1-phosphate (S1P) in a mixed-type manner ($K_i \sim 10^{-7}$ M). The homologous ecto-phosphodiesterase NPP1, which lacks lysophospholipase D activity, is insensitive to LPA and S1P. Our results suggest that, by repressing ATX activity, LPA can regulate its own biosynthesis in the extracellular environment, and they reveal a novel role for S1P as an inhibitor of ATX, in addition to its well established role as a receptor ligand.

Autotaxin (ATX)[1] is a member of the nucleotide pyrophosphatase/phosphodiesterase (NPP) family of ecto-enzymes that hydrolyze phosphodiester bonds in various nucleotides and nucleotide derivatives (1–3). ATX, also termed NPP2, was originally isolated as an autocrine motility factor for melanoma cells (4, 5) and later found to enhance the invasive and metastatic potential of Ras-transformed NIH3T3 cells in nude mice and to induce an angiogenic response in Matrigel plug assays (6, 7). ATX mRNA is overexpressed in various human cancers, adding support to a link between ATX and tumor progression (8). Expression analysis has further suggested a normal physiological role for ATX in neurogenesis, oligodendrocyte differentiation, and myelination (9, 10).

The mode of action of ATX/NPP2 has long been elusive because the biological effects of ATX could not be explained by nucleotide hydrolysis. The surprise came when it was discovered that ATX is identical to plasma lysophospholipase D (lyso-PLD) and acts by hydrolyzing lysophospatidylcholine (LPC) into lysophosphatidic acid (LPA) (11, 12), a lipid mediator that signals cell proliferation, migration, and survival via specific G protein-coupled receptors (13). It has now become clear that *de novo* production of LPA can fully account for the biological effects of ATX observed in cell culture. The lysophospholipid substrate range of ATX has recently been broadened by showing that the enzyme can also hydrolyze sphingosylphosphorylcholine (SPC) to yield sphingosine 1-phosphate (S1P) (14), a bioactive lipid with signaling properties very similar to those of LPA while acting on distinct receptors (15–17). The physiological significance of the SPC-to-S1P conversion is debatable, however, because the reported K_m of ATX for SPC (14) is 3 orders of magnitude higher than the normal SPC levels in plasma and serum (18). Rather than through SPC hydrolysis, S1P is thought to originate largely from the phosphorylation of sphingosine by sphingosine kinases (19).

Mutational analysis has revealed that the lyso-PLD and nucleotide phosphodiesterase activities of ATX originate from the same catalytic site (20, 21). Unexpectedly, the other two members of the NPP family (NPP1 and NPP3) lack intrinsic lyso-PLD activity despite their close homology to ATX (21). Given the differences in substrate specificity, it is not surprising that the NPPs appear to have largely unrelated physiological functions. The founding member, NPP1, hydrolyzes ATP into pyrophosphate, an inhibitor of calcification, and thereby regulates bone mineralization, whereas the third member, NPP3, promotes differentiation and invasion of glial cells by an unknown mechanism (3).

An unresolved question concerns the regulation of ATX activity. One puzzling observation is that LPA levels in plasma or freshly isolated blood are very low (22–24), yet plasma ATX is constitutively active and its substrate LPC abundantly present (> 100 μM) (25). This suggests that ATX is negatively regulated *in vivo*, but physiological or pharmacological inhibitors of ATX have not been identified to date. In the present study we sought to examine how ATX activity is regulated in the extracellular milieu. To this end, we used a newly invented fluorescence resonance energy transfer (FRET)-based phosphodiesterase sensor (termed CPF4; see Ref. 26) that, as we show here, reports ATX activity in conditioned media with superior sensitivity. Using this assay system, we demonstrate that ATX,

* This work was supported by the Dutch Cancer Society. The costs of publication of this article were defrayed in part by the payment of page charges. This article must therefore be hereby marked "*advertisement*" in accordance with 18 U.S.C. Section 1734 solely to indicate this fact.

[S] The on-line version of this article (available at http://www.jbc.org) contains supplemental Fig. 1.

** To whom correspondence should be addressed. Tel.: 31-20-512-1971; Fax: 31-20-512-1989; E-mail: w.moolenaar@nki.nl.

[1] The abbreviations used are: ATX, autotaxin; BSA, bovine serum albumin; FRET, fluorescence resonance energy transfer; LPA, lysophosphatidic acid; LPC, lysophosphatidylcholine; NPP, ectonucleotide pyrophosphatase/phosphodiesterase; PLD, phospholipase D; lyso-PLD, lysophospholipase D; SPC, sphingosylphosphorylcholine; S1P, sphingosine 1-phosphate; pNP, *para*-nitrophenolate; pNP-TMP, *para*-nitrophenyl thymidine-5′-monophosphate; bis-pNPP, bis(*para*-nitrotrophenyl) phosphate; GFP, green fluorescent protein; HA, hemagglutinin.

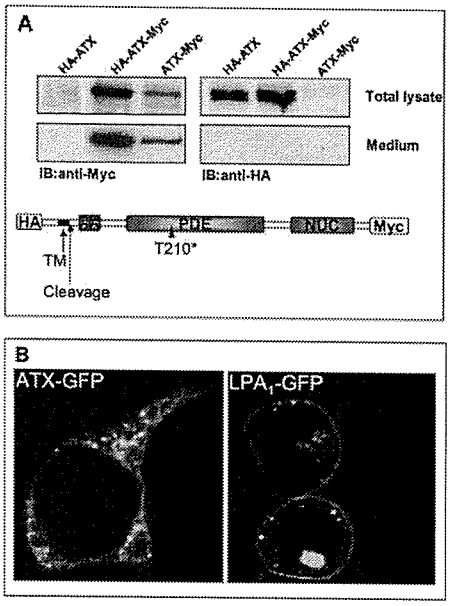

FIG. 1. **ATX processing and secretion.** *A*, human full-length ATX was expressed in HEK293T cells as a fusion protein with an N-terminal HA tag and/or a C-terminal Myc tag, as indicated. ATX expression in cell lysates and conditioned medium was analyzed by Western blotting using antibodies against the HA and Myc epitopes. Equal amounts of cell lysate and medium were applied in each experiment. HA-ATX is undetectable in the medium, consistent with N-terminal cleavage prior to secretion. *IB*, immunoblot; *TM*, transmembrane domain; *SO*, somatomedin-like domain; *PDE*, phosphodiesterase domain; *NUC*, nuclease-like domain. threonine residue (*T210*) is essential for catalytic activity. *B*, subcellular localization of ATX and the LPA_1 receptor (both C-terminally fused to GFP) in HEK293T cells. Unlike LPA_1, ATX is not detected at the cell surface but, instead, localizes to intracellular vesicles and reticular structures. Cells transfected with ATX-GFP or LPA_1-GFP (28) were fixed with ice-cold methanol at 24 h after transfection.

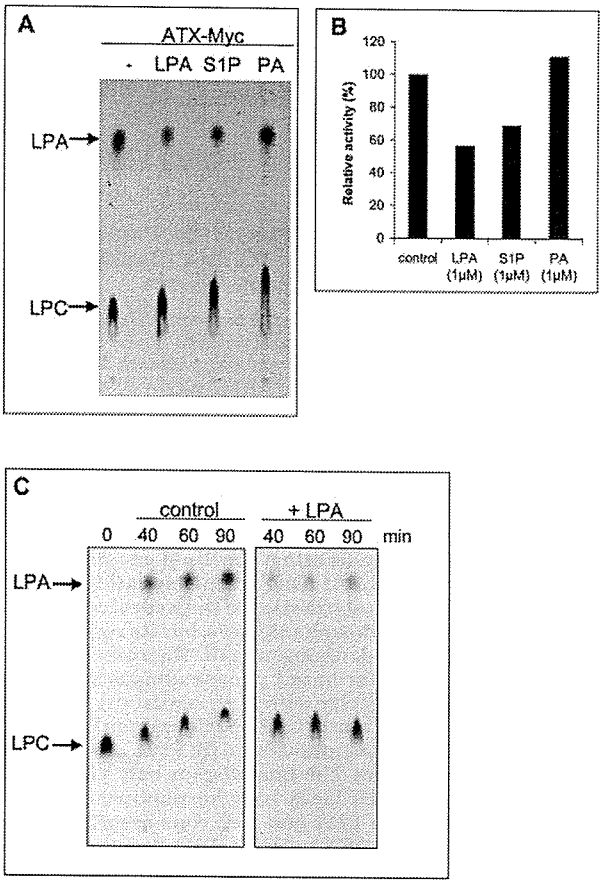

FIG. 2. **lyso-PLD activity of ATX.** *A*, lyso-PLD activity. Hydrolysis of 1-[1-^{14}C]palmitoyl-LPC into LPA by ATX-Myc in conditioned medium was analyzed by thin layer chromatography. The concentration of unlabeled LPC was 1 μM. The reaction was terminated after 2 h. LPC and LPA standards were run separately (not shown). LPA, S1P, and phosphatidic acid (*PA*) were added at 1 μM. *B*, graphical representation of data from two independent thin layer chromatography assays. *C*, time course of LPC hydrolysis into LPA and inhibition by LPA, added at 1 μM.

secreted by the classical export route, is potently and specifically inhibited by LPA and S1P at biologically relevant concentrations. These results have important implications for lysophospholipid action and signaling in general and ATX targeting in particular.

EXPERIMENTAL PROCEDURES

Cell Culture and Materials—HEK293T cells were grown in Dulbecco's modified Eagle's medium containing 10% fetal calf serum. All phospholipids were obtained from Avanti Polar Lipids Inc. (Alabaster, AL). Brefeldin A, monensin, BSA, fatty acid-free BSA (99%), *para*-nitrophenyl thymidine-5′-monophosphate (pNP-TMP), and bis(*para*-nitrotrophenyl) phosphate (bis-pNPP) were from Sigma. Highly purified PLD from *Streptomyces chromofuscus*, sphingomyelinase D from *Loxosceles laeta*, and sphingomyelinase D from *Corynebacterium pseudotuberculosis* were kindly provided by M. Roberts (Boston College), D. Tambourgi (Instituto Butantan, Sao Paulo, Brazil), and S. Billington (University of Arizona), respectively.

cDNA Cloning—RNA extracted from human diploid foreskin fibroblasts was used to generate cDNA using Invitrogen reverse transcriptase. ATX cDNA was isolated using ATX-specific primers. The stop codon was removed and KpnI and NotI restriction sites were introduced at the 5′ and 3′ sites, respectively. After digestion, ATX was ligated in pcDNA3 vector with 3′ Myc tag (ATX-Myc), 5′ HA tag (HA-ATX), or 5′ HA tag and 3′ Myc tag (HA-ATX-Myc), and in pEGFP-N3 (ATX-GFP). Sequencing showed that the ATX inserts were identical to human ATX (GenBank™ accession number BC034961). The catalytically inactive mutant ATX(T210A) (27) was generated using the Stratagene site-directed mutagenesis kit.

Transfection and Western Blotting—HEK293T cells were transfected with ATX constructs using the calcium phosphate method. At 24 h after transfection, cells were exposed to serum-free Dulbecco's modified Eagle's medium for 30 h. Conditioned medium was centrifuged (5000 rpm for 30 min) to remove cell debris. Medium was used without further purification and analyzed for the presence of ATX by Western blotting and activity assays. There was very little variation in ATX activity between different batches of conditioned medium. For Western blot analysis, nitrocellulose filters were blocked using 5% nonfat powdered milk and probed with primary antibodies (9E10 anti-Myc and 3F10 anti-HA; Roche Applied Science) and horseradish peroxidase-conjugated secondary antibodies (Dako, Glostrup, Denmark). Proteins were visualized using the ECL detection system (Amersham Biosciences).

Recombinant ATX—The Bac-to-Bac baculovirus expression system (Invitrogen) was used for ATX production. ATX cDNA fused to the honeybee melittin signal sequence at the 5′ end was cloned into the pFastBac I vector (Invitrogen). The resulting plasmid was then used for generating recombinant baculovirus to infect Sf9 insect cells, which were grown in SF-900 II medium (Invitrogen); the multiplicity of infection was ~5. After 60 h of infection, medium containing secreted ATX was collected by low speed centrifugation and applied onto a Q-Sepharose column (Amersham Biosciences). The flow-through was applied onto a hydroxyapatite column (Bio-Rad), and the bound proteins were eluted with a linear potassium phosphate gradient. The ATX-containing fractions were applied onto an isopropyl column (Amersham Biosciences), and bound proteins were eluted with a decreasing linear gradient of ammonium sulfate. Purity of ATX-containing fractions was > 95% as shown by SDS-PAGE and Coomassie Blue staining. The approximate yield was about 3 mg of pure protein from 10 liters of culture supernatant.

Recombinant NPP1—A soluble secreted form of human NPP1 was made by in-frame ligation of its extracellular domain to the BamHI site